



Article

Associated Effects of Sodium Chloride and Dihydrate Gypsum on the Mechanical Performance and Hydration Properties of Slag-Based Geopolymer

Quan Shen ^{1,2}, Benxiao Li ² , Wei He ^{2,*} , Xia Meng ³ and Yinlan Shen ⁴¹ Shanghai Interlink Road & Bridge Engineering Co., Ltd., Shanghai 201213, China; shenquansh@163.com² School of Civil and Transportation Engineering, Beijing University of Civil Engineering and Architecture, Beijing 100044, China; libxhi@foxmail.com³ Architectural Design and Research Institute of Tsinghua University Co., Ltd., Beijing 100084, China; mengxia@thad.com.cn⁴ Faculty of Architecture, Civil and Transportation Engineering, Beijing University of Technology, Beijing 100124, China; shenyinlan@bjut.edu.cn

* Correspondence: hewei@bucea.edu.cn

Abstract: The associated effect of sodium chloride and dihydrate gypsum on the mechanical performance of a slag-based geopolymer activated by quicklime was investigated by compressive strength, shrinkage, and square circle anti-cracking tests of mortar with a 0.5 water–binder ratio and a 1:3 binder–sand ratio, as well as paste soundness, powder X-ray diffraction (XRD), thermogravimetric analysis (TGA), scanning electron microscopy with energy dispersive spectroscopy (SEM-EDS), and mercury intrusion porosimetry (MIP) of the paste. The results indicate that (1) when dihydrate gypsum is used alone, it combines with calcium aluminate hydrate (C-A-H) to form calcium sulfoaluminate hydrate (AFt), which encourages the hydration process of slag. A 7.5% addition can result in an increase of 97.33% and 36.92% in 3-day and 28-day compressive strengths, respectively. When NaCl is used by itself, it facilitates the condensation of the aluminum silicate tetrahedron unit and generates zeolite. A 2% dosage can lead to a 66.67% increase in the 3-day compressive strength, while causing a 15.89% reduction in the 28-day compressive strength. (2) The combined effect of 2% NaCl and 7.5% gypsum results in the formation of needle-like and rod-shaped AFt, Friedel’s salt, and plate-like Kuzel’s salt in the geopolymer. This leads to an increase in 3-day and 28-day compressive strengths by 148% and 37.85%, respectively. Furthermore, it reduces the porosity by 18.7%. (3) Both NaCl and gypsum enhance the paste soundness of the slag-based geopolymer, and they do no harm to the crack resistance of the geopolymer. The drying shrinkage of the geopolymer at 28 days is just 0.48×10^{-3} , which is only 66.7% of OPC. This slag-based geopolymer has a simple preparation process, good volume stability, low raw material cost, low energy consumption, and low carbon emissions. It can be used instead of 32.5 slag Portland cement in plain concrete applications, and has high engineering, economic, and environmental values.

Keywords: sodium chloride; dihydrate gypsum; slag-based geopolymer; mechanical performance; hydration mechanism; Friedel’s salt; Kuzel’s salt



Citation: Shen, Q.; Li, B.; He, W.; Meng, X.; Shen, Y. Associated Effects of Sodium Chloride and Dihydrate Gypsum on the Mechanical Performance and Hydration Properties of Slag-Based Geopolymer. *Buildings* **2023**, *13*, 1285. <https://doi.org/10.3390/buildings13051285>

Academic Editors: Shan Gao, Jingxuan Wang, Dewen Kong and Yong Liu

Received: 10 April 2023

Revised: 30 April 2023

Accepted: 11 May 2023

Published: 15 May 2023



Copyright: © 2023 by the authors. Licensee MDPI, Basel, Switzerland. This article is an open access article distributed under the terms and conditions of the Creative Commons Attribution (CC BY) license (<https://creativecommons.org/licenses/by/4.0/>).

1. Introduction

The worldwide construction sector bears the onus of generating 39% of CO₂ emissions and depleting over 50% natural resources extracted [1], and cement manufacturing is directly responsible for approximately 5% of artificial CO₂ emissions, with 0.8–1.1 tons of CO₂ released against each ton of cement production [2]. Geopolymers are one of the several alternative cementitious materials to Portland cement being investigated. They are formed by the alkaline activation of industrial solid wastes, such as slag, steel slag, fly ash [3], red mud [4], as well as natural pozzolan [5]. Their preparation process has low energy

consumption and low emissions, so the advantages of geopolymers fit well with China's strategic goals of "carbon peak and carbon neutrality" [6]. Additionally, geopolymers have exceptional characteristics, such as fast setting and hardening, high strength [7,8], resistance to high temperature [9] and acid corrosion [10–13], excellent impermeability [14], and good freeze–thaw resistance [15–17]. They can recycle industrial solid waste and have great potential for use in various applications.

Traditional slag-based geopolymers usually require a strong alkaline activator. Although they have a remarkable activation effect, they have several drawbacks, including over-rapid early-stage strength formation, low later-stage strength potential, and severe shrinkage. The shrinkage of alkali-activated slag concrete is generally at least twice that of ordinary Portland cement concrete, and the shrinkage of alkali-activated slag mortar activated by sodium hydroxide and water glass is three and six times that of ordinary Portland cement [18–22], respectively. Currently, it is widely believed that the high gel content of geopolymers and the excessively high proportion of pores smaller than 10 nm cause significant negative pore pressure during dehydration, resulting in excessive shrinkage [23].

Cheng et al. [24] found that the addition of NaCl at a dosage between 0% and 5% resulted in a greater improvement in the strength of slag-based geopolymers. However, when the NaCl content exceeded 5%, the strength increase in slag-based geopolymers becomes lower. Lv et al. [25] observed that the addition of 1% NaCl increased the strength of fly-ash-based geopolymer, but when the NaCl content is 3–11%, the strength of fly-ash-based geopolymers drops. Cao et al. [26] also found that adding 1% NaCl accelerated the hydration process of cement. He et al. [27] discovered that increasing the NaCl level to 2% increased the strength of slag-based geopolymers. Liu et al. [28] discovered that the geopolymer strength is greatest when the gypsum component is 10%. Zhang et al. [29] found that the strength of geopolymer mortar increased when adding less than 2% gypsum and decreased significantly when adding 5% gypsum. Xing et al. [30] found that the compressive strength of the geopolymer test block is the greatest when the gypsum component is 10%.

Previous studies [25,31–33] used a composite activator consisting of light calcined magnesia (MgO), sodium chloride (NaCl), building gypsum, and quicklime (CaO) to activate slag. During the hydration process, abundant crystalline hydration products, such as Fredel's salt, Kuzel's salt, and Aft, filled the gel pores, while MgO compensated for the shrinkage. The geopolymer met the strength requirements of 32.5 slag Portland cement. However, MgO is costly and limits its application potential. So, in this study, we removed the MgO component and used more gypsum and quicklime to compensate for shrinkage. By adjusting, it can further reduce energy consumption and emissions and be cheaper than OPC and strong alkali-activated slag-based geopolymer. The mechanical properties of this geopolymer were investigated by the compressive strength, square circle anti-cracking tests of mortar, and soundness of paste, and its microscopic mechanism was studied using XRD, SEM, TGA, and MIP. The differences in shrinkage between this geopolymer and P.O. 42.5 cement were also compared to comprehensively evaluate the performance of the slag-based geopolymer and provide theoretical support for its application in concrete engineering, especially in plain concrete engineering. The research of the composite-activated slag-based geopolymer has positive significance for reusing granulated blast-furnace slag and reducing carbon emissions caused by cement production.

2. Materials and Methods

2.1. Materials

The slag utilized in this paper is S95 slag powder manufactured by Hebei JINTAICHENG Environmental Resources Co., Ltd., Xingtai, China, with a density of 2.87 g/cm³. Chemical compositions were analyzed using XRF, and the instrument used was Japanese Rigaku Supermini 200. The specific surface area and particle size distribution were analyzed using a Laser Diffraction Particle Size Analyzer. The instrument used was Mastersize 3000-F made by Malvern Panalytical. The results are shown in Table 1, Table 2, and Figure 1, respectively.

The slag's chemical module was $K = 2.17$; alkalinity modules were $Mo = 1.14$; and the observed 28-days activity coefficient was 95. The XRD spectrum shown in Figure 2 clearly exhibits a 'steamed bread peak', suggesting the presence of amorphous phase minerals in the slag, primarily active SiO_2 and active Al_2O_3 [34].

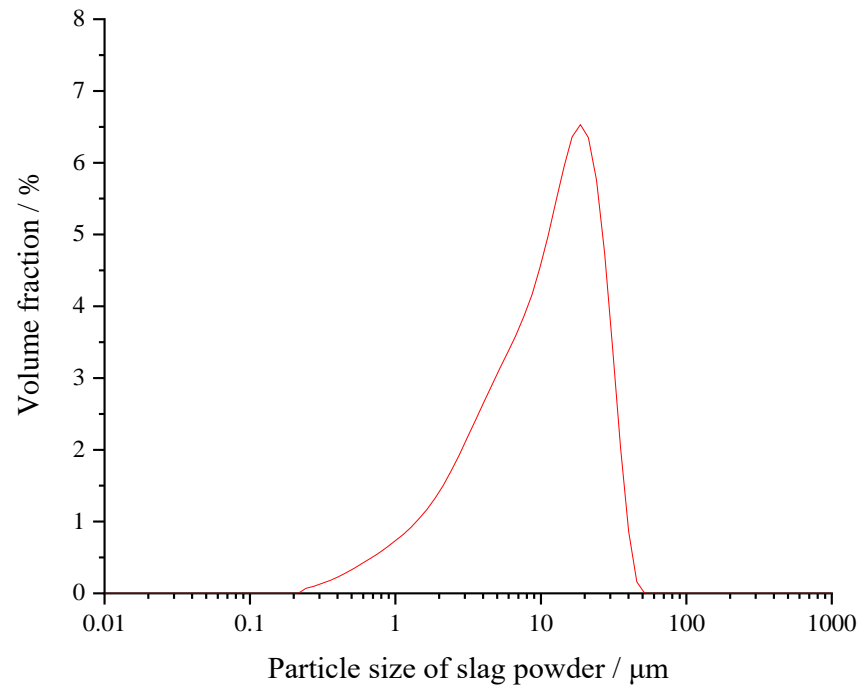


Figure 1. Particle size distribution curve.

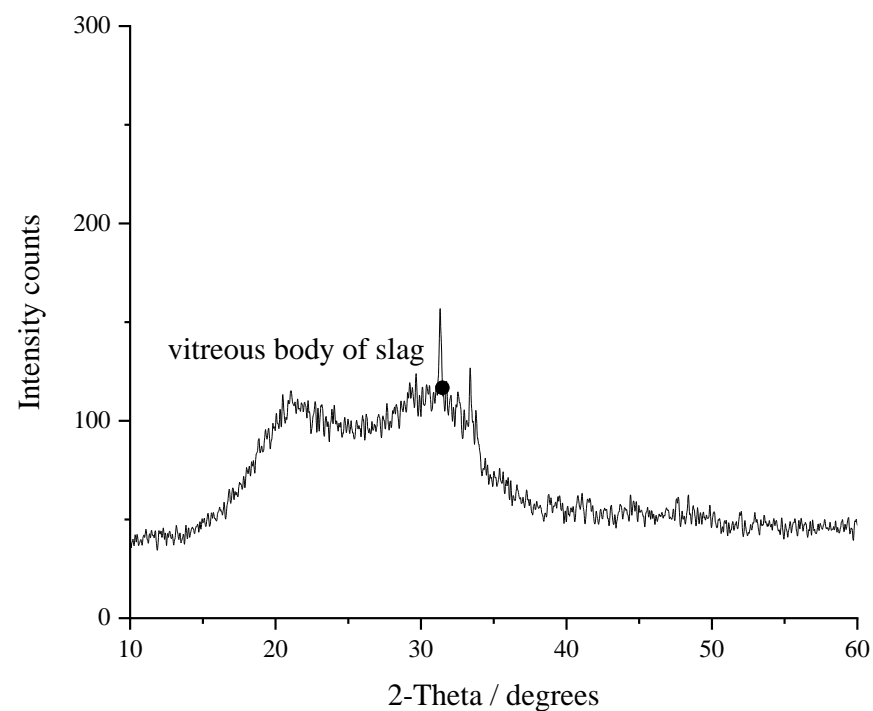


Figure 2. X-ray diffraction spectra of the slag.

Table 1. Chemical composition of slag (mass %).

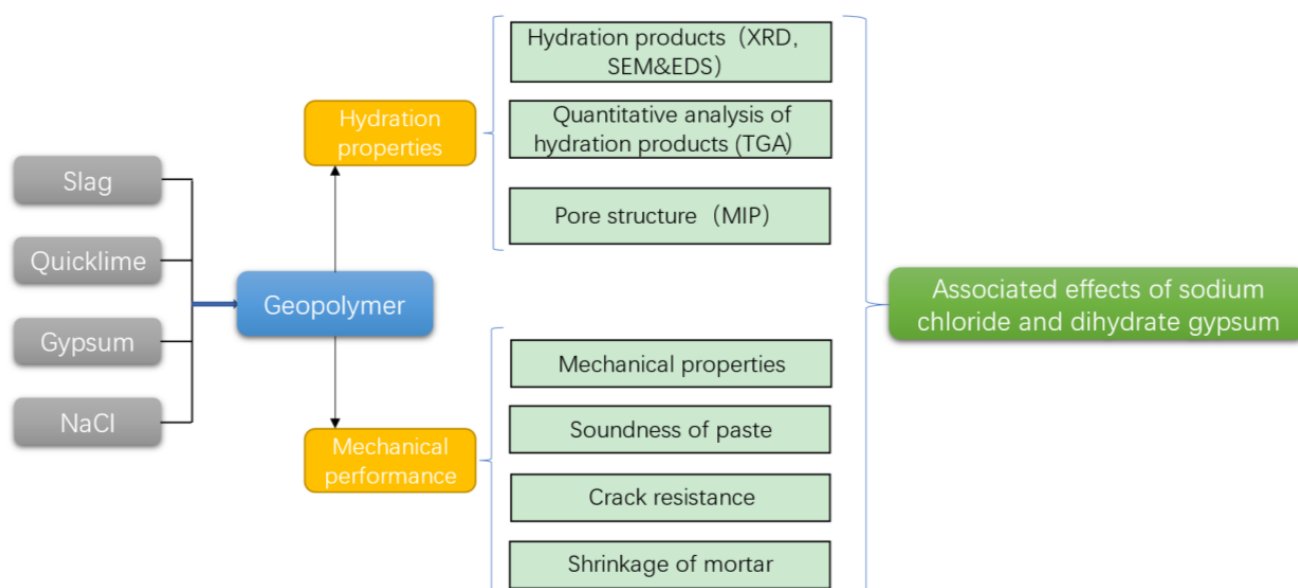
SiO ₂	Al ₂ O ₃	SO ₃	MgO	CaO	Fe ₂ O ₃	Na ₂ O	K ₂ O
27.56	15.80	2.89	7.52	42.19	0.31	0.45	0.45
Cl	P ₂ O ₅	TiO ₂	MnO	SrO ₂	Y ₂ O ₃	Others	
0.09	0.05	1.97	0.61	0.09	0.01	0.01	

Table 2. Particle size distribution.

Specific Surface Area	Dx (10)	Dx (50)	Dx (90)
432.9 m ² /kg	2.23 μm	12.0 μm	28.3 μm

Tianjin BEICHEN, Tianjin BEILIAN, and Tianjin ZHIYUAN Chemical Industry provided the analytical pure NaCl (>99.9%), dihydrate gypsum (CaSO₄·2H₂O) (>99.9%), and quicklime (>99.9%) employed in the experiment, respectively. Quicklime reacts with water to form calcium hydroxide, which increases the alkalinity of the gelling system and plays the role of an alkaline activator. Xiamen AISOU standard sand Co., Ltd., Xiamen, China manufactured the ISO standard sand. A comparison experiment was carried out with 42.5 ordinary Portland cement produced by Beijing JINYU Group Co., Ltd., Beijing, China, with a specific surface area of 349.8 m²/kg, to assess the volume stability difference between the compound slag-based geopolymer and ordinary Portland cement.

The flowchart of this study is shown in Figure 3.

**Figure 3.** Flowchart of the research.

2.2. Experiment Methods

Although NaCl and gypsum have overlapping reactants in slag-based geopolymers activated by NaCl, gypsum, and quicklime, they are also distinct, and the composite application can give superior results. Based on previous experiments, the strength is stronger when the composite activator content is 25%. Therefore, under the condition of 25% activator content, the NaCl dosage was set at 2%, 4%, and 6%, marked as L, M, and H, respectively; the gypsum dosage was set at 2.5%, 5%, 7.5%, and 10%, represented by A, B, C, and D, respectively. The effects of NaCl and gypsum on slag-based geopolymer characteristics were investigated. The test group LC with the highest strength was chosen as the control group without NaCl (0C), without gypsum (L0), and neither NaCl nor gypsum

(OQ, only quicklime) by replacing the NaCl and gypsum components with quicklime in order to study the activating mechanism of NaCl and gypsum. The amount of activators in the LC group was adjusted to 20%, 30%, and 35%, and the optimum activator dose was tested. Because conventional geopolymer has a far higher dry shrinkage than Portland cement, it can cause interior micro fractures and strength degradation [18].

The calcium oxide level was relatively low, and the alkaline environment that may be created was restricted. Previous research had also shown that the excitation process takes longer with this excitation combination, so the 28-day strength of geopolymer under compound activators may be insufficient; therefore, a 56-day strength test was performed for the LC group. The volume stability of the geopolymer was compared with a P.O. 42.5 cement control group (OPC). Mixture proportions are detailed in Table 3. The reaction mechanism of the compound slag-based geopolymer activated by quicklime was analyzed, the law of mechanical properties was studied, and the volume stability was compared and evaluated by studying the products, pore structure, and mortar strength of the composite system of NaCl, gypsum, quicklime, and slag with different ratios and comparing the stability, shrinkage, and crack resistance of the paste. The reaction mechanism is comparable for the test groups with the same composition and little change in dose, and the test group with high strength as well as good volumetric stability (or not) has research value. As a result, the conventional test group and the control group are primarily investigated. In Table 3, a checkmark (✓) indicates that this set of tests was performed, whereas a slash (/) indicates that it is not within the scope of the research.

Table 3. Mixture proportions (SC, NaCl; DG, dihydrate gypsum; QL, quicklime; AT, activator/%).

No.	Ratio	SC	DG	QL	AT	Slag	Paste			Mortar	
							Micro-Test	Soundness	Strength	Shrinkage	Cracking
1	LA	2	2.5	20.5	25	75	/	✓	✓	/	/
2	LB	2	5	18	25	75	/	✓	✓	/	/
3	LC	2	7.5	15.5	25	75	✓	✓	✓	✓	✓
4	LD	2	10	13	25	75	/	/	✓	/	/
5	MA	4	2.5	18.5	25	75	/	/	✓	/	/
6	MB	4	5	16	25	75	/	/	✓	/	/
7	MC	4	7.5	13.5	25	75	/	/	✓	/	/
8	MD	4	10	11	25	75	/	/	✓	/	/
9	HA	6	2.5	16.5	25	75	/	/	✓	/	/
10	HB	6	5	14	25	75	/	/	✓	/	/
11	HC	6	7.5	11.5	25	75	/	/	✓	/	/
12	HD	6	10	9	25	75	/	/	✓	/	/
13	OC	0	8	17	25	75	✓	✓	✓	/	✓
14	L0	3	0	22	25	75	✓	✓	✓	/	✓
15	OQ	0	0	25	25	75	✓	✓	✓	/	✓
16	LC 20%	1.5	6	12.5	20	80	/	/	✓	/	/
17	LC 30%	2.5	9	18.5	30	70	/	/	✓	/	/
18	LC 35%	3	11	21	35	65	/	/	✓	/	/

(1) Micro-tests of Hardened paste

A pure paste sample was made with a 0.35 water–binder ratio and placed in a test tube for standard curing. The sample was taken out at the age of 3 and 28 days and split into little pieces before being sealed in a test tube containing anhydrous ethanol to stop hydration. The samples were collected from a sealed anhydrous ethanol test tube and vacuum-dried for 24 h at 60 °C for tests in the LC test group as well as the OC, L0, and OQ control groups.

a. X-ray diffraction (XRD)

The paste sample was ground using a mortar until there was no particle sensation and then passed through a 45 µm sieve. The groove on the diffractometer sample table was filled with the sieved paste powder. To scan the phase, a Cu target was used with a tube

voltage of 40 kV, a tube current of 40 mA, a scanning speed of 6 °/min, and a test range of 3 to 80°.

b. Thermogravimetric analysis (TGA)

The AFt, $\text{Ca}(\text{OH})_2$, and chemical bonding water of the samples were evaluated by mass changes with temperature after being heated from 30 °C to 1000 °C at 10 °C/min in a nitrogen environment.

c. Scanning electron microscopy with energy dispersive spectroscopy (SEM-EDS)

The microstructure of the shattered sample was examined using a ZEISS Gemini 300 scanning electron microscope, manufactured by Zeiss, Germany, after a portion of it was sprayed with carbon.

d. Mercury intrusion porosimetry (MIP)

The mercury injection experiment technique involves calculating the diameter and volume of various-sized holes based on the functional connection between the amount of mercury injected into the hardened paste and the applied pressure. The fractal dimension of pore volume may be determined directly from the experimental data of mercury intrusion porosimetry based on the variable features of pore volume and pore diameter. The curves are displayed after calculating the logarithms of dV/dr and dr , and the fractal dimension of the pore volume is estimated using the slope of the curve.

(2) Soundness of paste

The SO_3 content of Portland cement specified in GB 175–2007 “Universal Portland Cement” standard is not more than 3.5%, mainly because of the potential risk of soundness caused by AFt. So, the pat paste was prepared in accordance with the measured standard consistency water consumption for study of soundness under standard curing conditions. Considering the mechanical properties and volume stability test results, LA, LB, LC, 0C, L0, and OQ test groups were selected for key research, and the cracking was observed and recorded regularly. The boiling test method was not used in the soundness test. AFt plays an important role in compensating for shrinkage and preventing cracking at the early stage of hardening, while AFt decomposes above 70 °C.

(3) Rupture and compressive strength tests of mortar

According to GB/T 17671-1999 test method for the strength of cement mortar (ISO method), 40 mm × 40 mm × 160 mm cement mortar samples were made with a 0.5 water–binder ratio and a 1:3 binder–sand ratio in line with Table 3. The rupture strength and compressive strength were measured after 3 and 28 days of curing.

(4) Shrinkage tests of mortar

The LC group with the highest strength was compared with grade 42.5 ordinary Portland cement. The mortar test blocks were prepared according to a binder–sand ratio of 1:3 and a water–binder ratio of 0.5. The drying shrinkage mortar samples were made in a 40 mm × 40 mm × 160 mm triple steel mold, and the plates at both ends of the mold have three 6 mm blind holes. A 25 mm long, 6 mm round head copper rod probe was placed before shaping, the surface was covered with a layer of the fresh-keeping film after forming, and it was placed in a standard curing room (temperature (20 ± 2) °C, relative humidity above 90%). The mold was removed after curing for 1 day, the initial value of the samples' length (accurate to 0.001 mm) was measured using a screw micrometer, the samples were placed on the confined frame, moved into the constant temperature and humidity room for curing (temperature (20 ± 2) °C, relative humidity $60\% \pm 5\%$), and the dial indicator readings of the samples at the age of 1 to 28 days were read. Paraffin wax was applied to the three removed mortar cubes, the interface was isolated with water in the air, and the autogenous shrinkage value was measured for 14 days under the same circumstances, as shown in Figure 4.

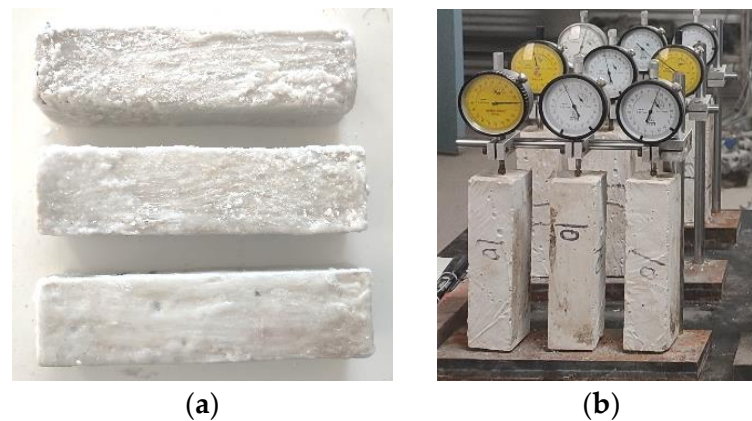


Figure 4. (a) Coated specimens with paraffin wax; (b) shrinkage test frame.

The autogenous and dry shrinkage strain values of each age was calculated according to the following formula:

$$\varepsilon = (l_0 - l_t) / l_0$$

where ε represents the value of shrinkage strain; l_0 is the initial length of the specimen; and l_t is the length of the specimen at the age of t days. The average value of the shrinkage strain of three specimens was taken for each ratio.

(5) Square circle anti-cracking tests of mortar

The traditional ring method is widely used in the early crack resistance test of concrete. The earliest ring-cracking method was proposed and applied by Carlson [35]. The ring device is composed of two steel rings. The uniform constraint on the specimen is realized by limiting the shrinkage of cement-based materials by the inner ring. However, the commonly used uniaxial constraint method is complex and cannot be compared in large quantities; the plate constraint method has some problems, such as uneven constraint. Therefore, this study adopts a new cracking evaluation model—square and circular anti-cracking mold—which can not only uniformly restrict the concrete sample but also crack the surface of the concrete sample within a certain time, so as to measure the crack length and width conveniently and quickly. The center of the square round anti-crack test mold used in this experiment is square, and the location of the crack is guided by the cube edges and corners, so as to observe the process of crack generation and propagation [36]. The outer ring diameter of the ring test mold used in the test is 210 mm, the inner ring diameter is 200 mm, the height is 100 mm, and the side length of the central square is 106.05 mm [37], as shown in Figure 5. The test samples were placed indoors, observed for 28 days, and the number and width of cracks were recorded.

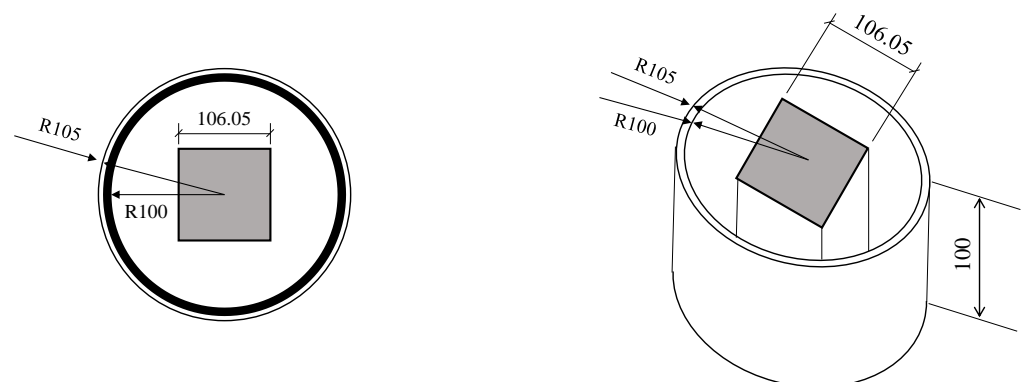


Figure 5. Square circle anti-cracking test mold.

3. Results and Discussion

3.1. Influence of NaCl and Gypsum on the Properties of Hardened Paste

To explore the hydration products and reaction process, the experimental groups LC, 0C, and L0 were principally investigated and compared to the control group OQ.

3.1.1. XRD

The hydration products of the geopolymer activated by quicklime, gypsum, and NaCl were analyzed using XRD, and the types of hydration products were obtained by qualitative analysis of the diffractogram, as shown in Figure 6.

In Figure 6, the LC group exhibits obvious diffraction peaks of $\text{Ca}(\text{OH})_2$, AFt ($3\text{CaO}\cdot\text{Al}_2\text{O}_3\cdot\text{CaSO}_4\cdot 12\text{H}_2\text{O}$), Friedel's salt ($3\text{CaO}\cdot\text{Al}_2\text{O}_3\cdot\text{CaCl}_2\cdot 10\text{H}_2\text{O}$), and Kuzel's salt ($3\text{CaO}\cdot\text{Al}_2\text{O}_3\cdot 0.5\text{CaCl}_2\cdot 0.5\text{CaSO}_4\cdot 12\text{H}_2\text{O}$), as well as unknown zeolite. Friedel's salt and Kuzel's salt are both double-layer metal hydroxides with positive charge on their laminates. To maintain overall electrical neutrality, a specific number of anions such as Cl^- and SO_4^{2-} are present between the laminates; at the same time, a particular number of water molecules are also present between layers [38,39]. The hydration of CaO generates $\text{Ca}(\text{OH})_2$, which subsequently reacts with slag to produce C-A-H. It then reacts with gypsum to form AFt. With time, the combined effect of NaCl and gypsum promotes the continued formation of Friedel's salt and Kuzel's salt, resulting in the enhancement of their diffraction peaks at 28 days. The diffraction peaks of Friedel's salt are found in the L0 group without adding gypsum because the slag includes a trace of SO_3 . In contrast, no diffraction peaks of Friedel's salt or Kuzel's salt were detected in the 0C group.

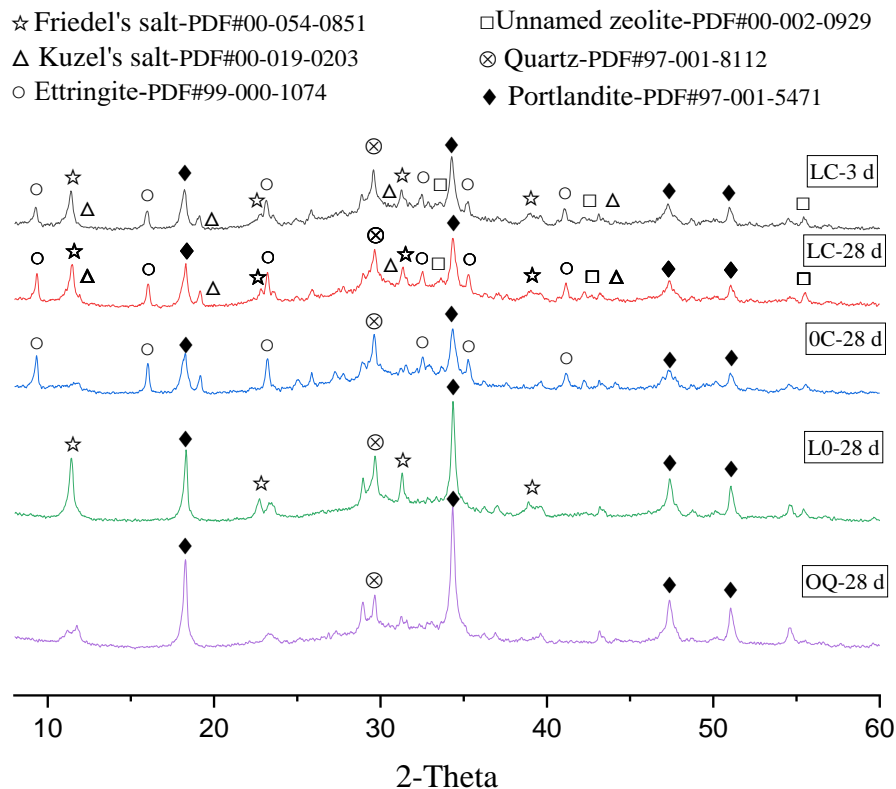
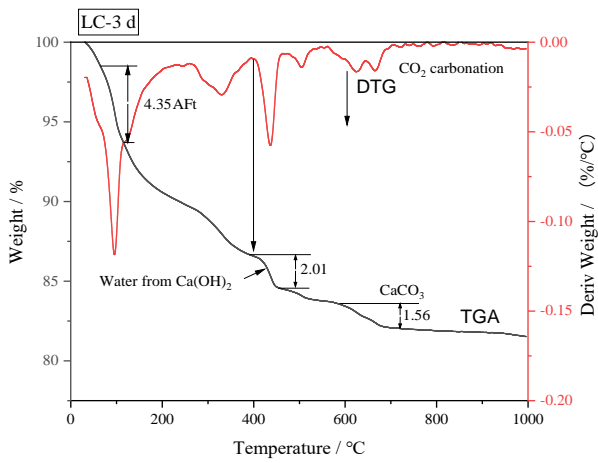


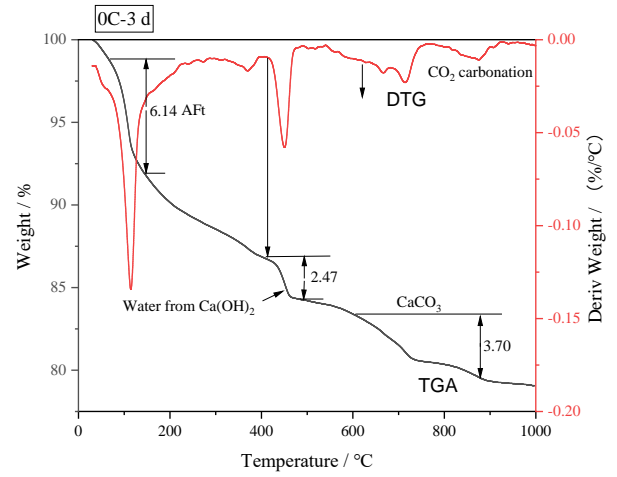
Figure 6. XRD pattern of geopolymer paste.

3.1.2. TGA

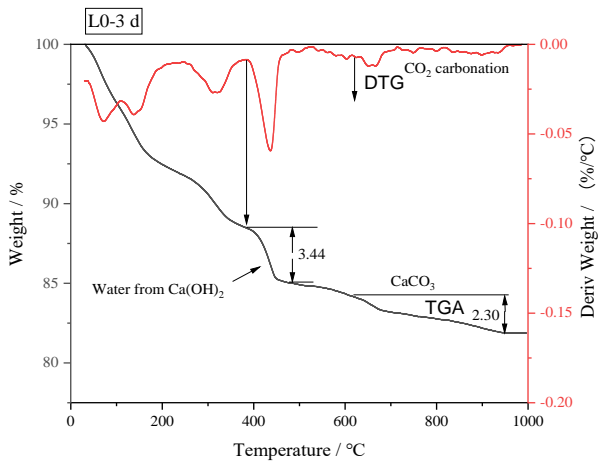
To quantify the influence of NaCl and gypsum on the hydration of slag, thermogravimetric analysis was carried out on the LC, 0C, L0, and OQ groups, and the TG-DTG curves are shown in Figure 7.



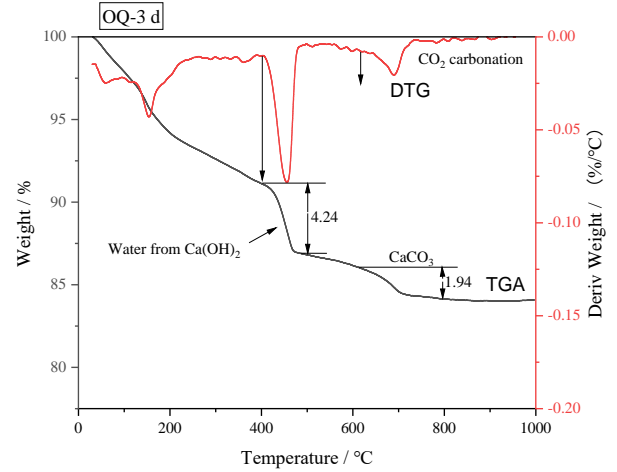
(a) LC-3 days



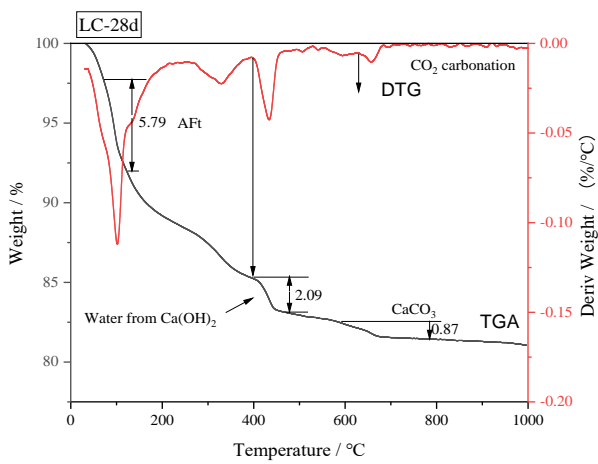
(b) OC-3 days



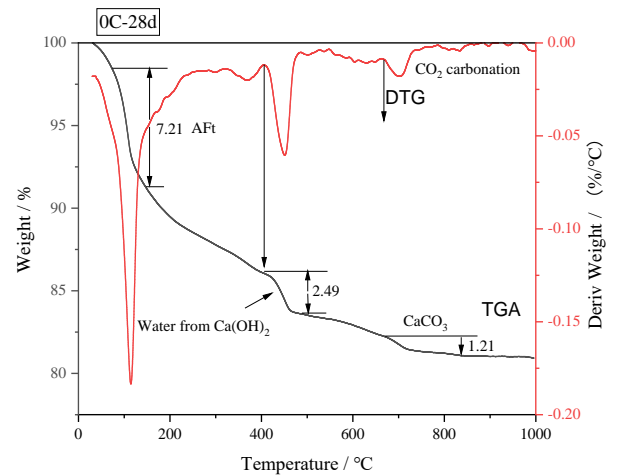
(c) L0-3 days



(d) OQ-3 days



(e) LC-28 days



(f) OC-28 days

Figure 7. Cont.

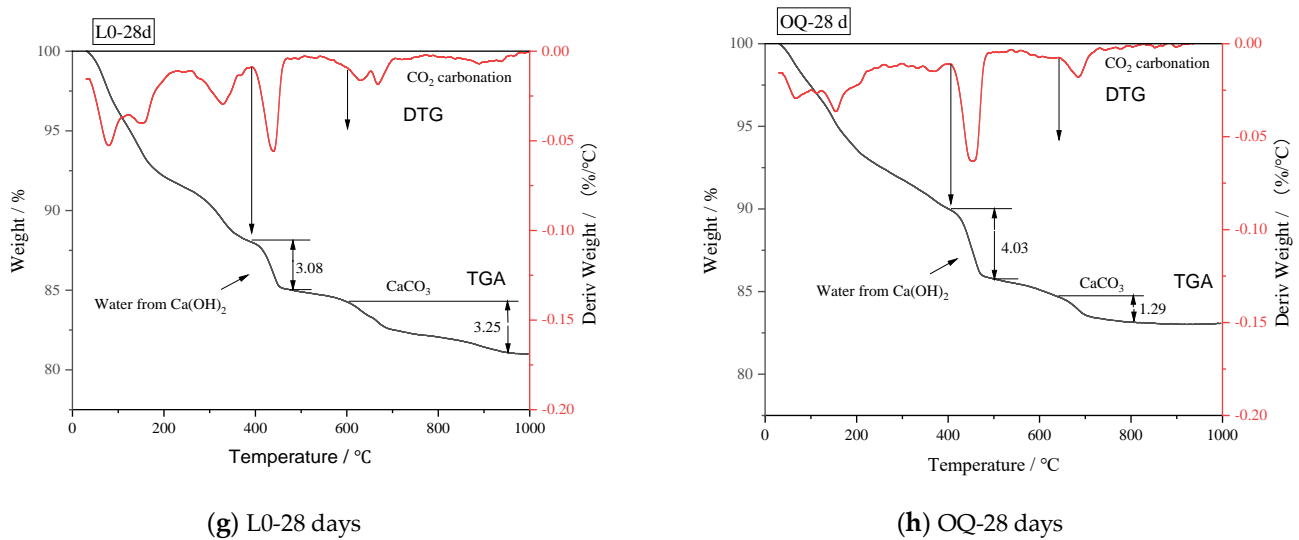


Figure 7. TG-DTG curves of geopolymer paste.

As shown in Figure 7, obvious AFt decomposition peaks occurring at 70~150 °C [40] can be seen in the OC and LC groups. Hydration of CaO produced $\text{Ca}(\text{OH})_2$, which can stimulate the activity of slag and promote hydration. As $\text{Ca}(\text{OH})_2$ acts as an activator in this process, a lower residual amount of $\text{Ca}(\text{OH})_2$ leads to a better slag hydration.

TG analysis can be used to determine the residual amount of $\text{Ca}(\text{OH})_2$, as it decomposes and releases water at 350 °C to 550 °C. Although the thermogravimetric loss of C-S-H can occur throughout the entire temperature range, certain inaccuracies in the predicted quantities of AFt and $\text{Ca}(\text{OH})_2$ cannot be measured. However, under the same conditions, measuring the relative concentration of $\text{Ca}(\text{OH})_2$ in each test group might still represent the degree of slag hydration. As the chemical bonding water content includes the water released by the thermogravimetric loss of $\text{Ca}(\text{OH})_2$, the hydration degree of slag must be subtracted from the quantity of water released by residual $\text{Ca}(\text{OH})_2$.

The amounts of AFt, $\text{Ca}(\text{OH})_2$, and chemical bonding water content are calculated and shown in Figure 8.

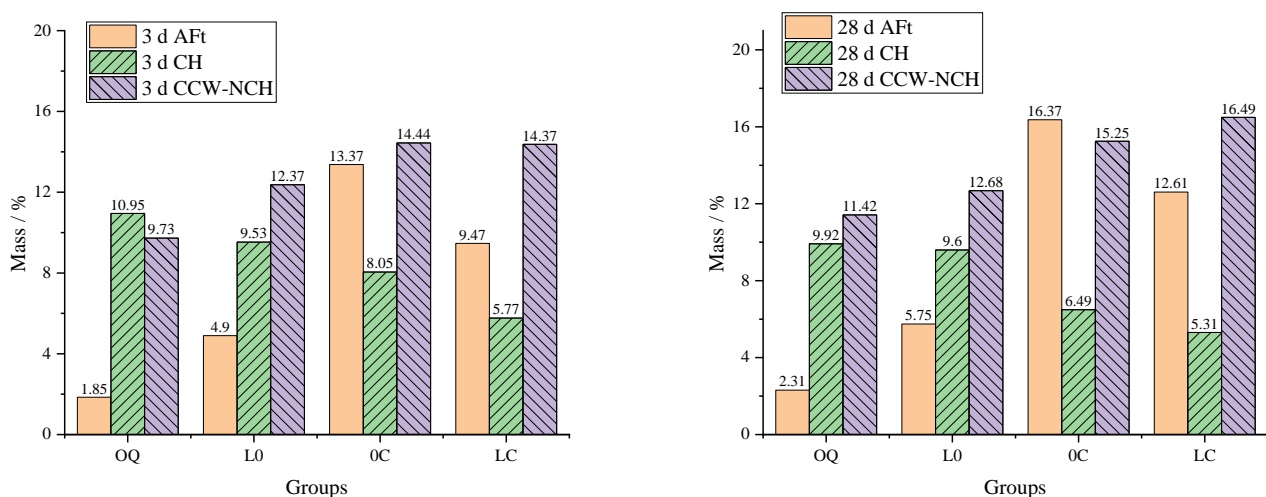


Figure 8. Percentage of AFt/CH/CCW-NCH (CCW-NCH deducts the amount of water released by the decomposition of $\text{Ca}(\text{OH})_2$ (CH)).

As shown in Figure 8, the CCW-NCH of the LO and OC groups are significantly higher than that of the OQ group at both 3 and 28 days, implying that sodium chloride and gypsum can effectively promote hydration individually. Furthermore, the CCW-NCH value of the

LC group is higher than both groups, demonstrating that the combined use of sodium chloride and gypsum results in a more pronounced promotion of hydration. Notably, the AFt contribution to CCW-NCH is relatively high in the 0C and L0 groups. AFt content in the LC group is 3.9% lower than 0C, suggesting that NaCl serves to boost slag hydration and reduce AFt formation. Moreover, the 28-day CCW-NCH increase is greater in the LC group than in the 0C group, thereby indicating that the addition of NaCl facilitates subsequent hydration enhancement. Within a few hours of mixing with water, AFt was produced, thereby improving early strength, while the formation of Freidel's salt and Kuzel's salt typically occurred later than that of AFt. The formation of Freidel's salt and Kuzel's salt consumed chloride ions, sulfate ions, and C-A-H, thereby reducing the formation of AFt in the hardened paste. There is no noticeable AFt decomposition peak observed in the OQ test group's DTG curve, which is attributed to the absence of gypsum. Furthermore, the $\text{Ca}(\text{OH})_2$ content of the 0C and L0 groups is lower than that of OQ, and the CCW-NCH content rose concomitantly, indicating that both gypsum and NaCl serve to enhance the reaction degree of slag. Finally, the LC group exhibits the greatest 28-day CCW-NCH content, indicating the highest reaction degree of slag and the most effective activation when NaCl and gypsum are used together.

NaCl reacts with the hydration products of slag to release NaOH, which further promotes the hydration of slag. The amount of chemically combined water in each group is increased after 28 days, compared to 3 days, indicating that the slag undergoes enhanced hydration over time, while the amount of $\text{Ca}(\text{OH})_2$ decreases. At 28 days, the $\text{Ca}(\text{OH})_2$ content of the LC group is 5.31%, meaning that 65.74% of the quicklime has engaged in the hydration process, thereby indicating that the amount of quicklime was sufficient.

3.1.3. SEM and EDS

The hydration products of the geopolymer were meticulously analyzed using SEM and EDS. The identification of the hydration products was based on their visual appearance and elemental composition, which are presented in Figures 9 and 10, as well as in Table 4.

Table 4. EDS analysis results of dots (atomic percentage).

Elements	Ca	Si	O	Al	S	Mg	Na	Cl
dot 1	20.90	6.16	58.23	2.34	3.38	1.49	1.57	1.33
dot 2	22.34	1.79	53.49	10.48	0.22	0.33	1.3	4.94
dot 3	13.49	4.64	59.27	3.22	1.08	0.75	3.43	1.10
dot 4	15.51	3.62	58.61	4.19	1.24	0.85	2.93	1.29

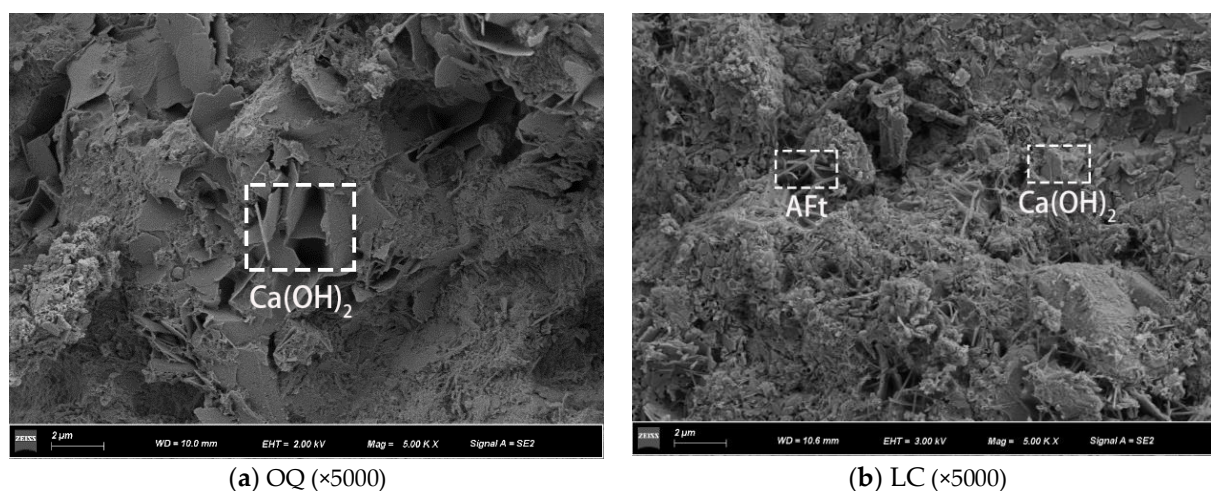


Figure 9. Cont.

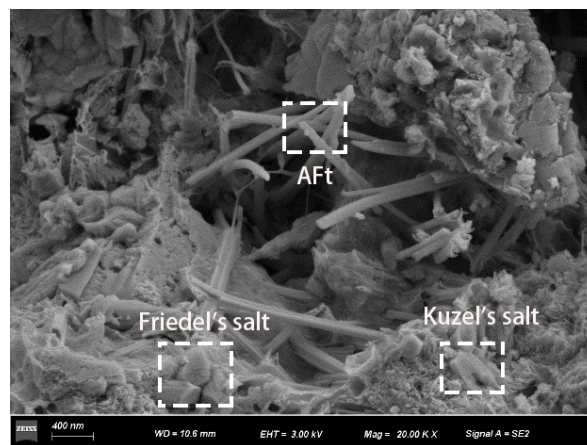
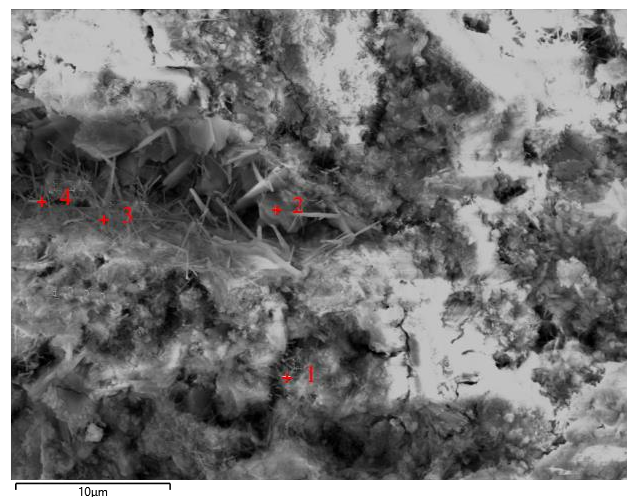
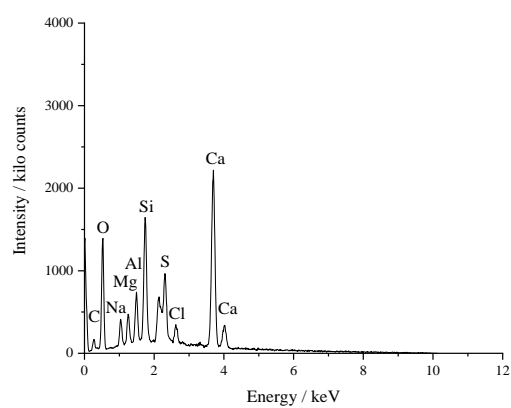
(c) LC ($\times 20,000$)

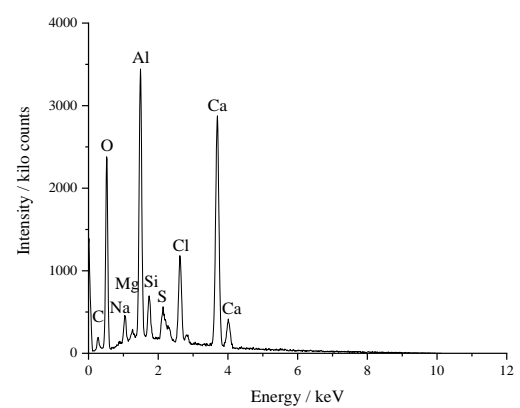
Figure 9. SEM images of the paste samples.



(a) Micrographs indicating the dot 1-4 locations of energy spectrum analysis.



(b) dot 1



(c) dot 2

Figure 10. Cont.

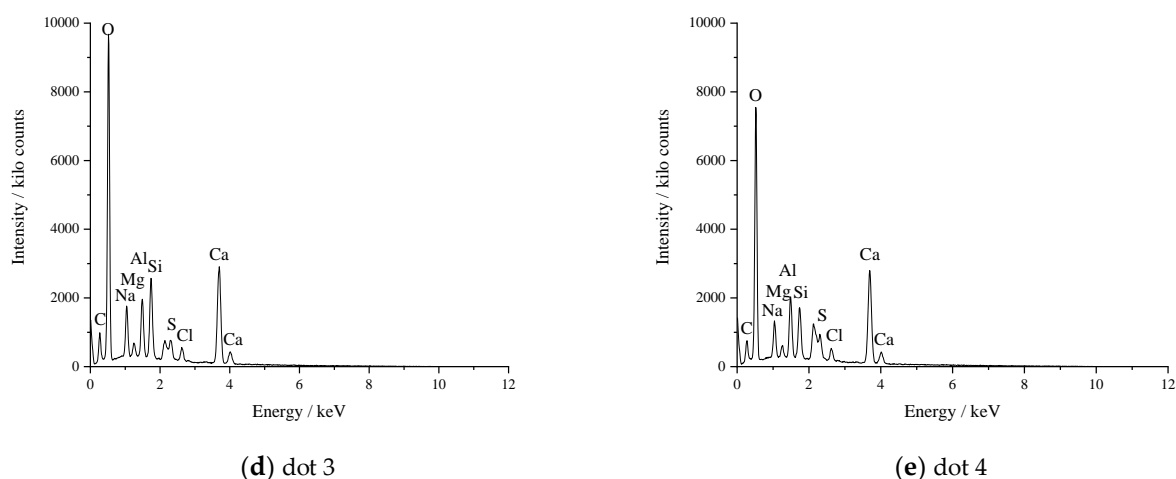


Figure 10. EDS spectra of geopolymer paste (the LC group).

It can be seen from Figure 10 and Table 4 that since the diameter of the determination point of the energy spectrum analysis may be larger than the size of the chlorine-containing compounds, the determination areas are mixed with other compounds, such as C-S-H gel, which may cause errors, so the influence of this part should be eliminated as much as possible. C-S-H gel has a calcium–silicon ratio that ranges between 0.8 and 2. It is assumed that the calcium–silicon ratio is constant and that all Si is present in the hydrated silica gel. After subtracting the calcium in the hydrated calcium silicate in Table 4, the Ca-Al-S-Cl ratio is recalculated to yield Table 5.

Table 5. Atom ratio.

Elements	Ca	Si	O	Al	S	Mg	Cl	Content
dot 1	4.95	0	24.2	2.34	0.67	0	1.33	KS
dot 2	12.16	0	31.24	5.48	0.00	0	4.94	FS
dot 3	6.53	0	40.78	3.22	1.08	0	1.10	AFt + FS
dot 4	8.08	0	39.39	4.19	1.24	0	1.29	AFt + FS

The combination of AFt, gypsum, portlandite, Friedel’s salt, and Kuzel’s salt with zeolite products (including Na and forsterite) can cause changes in the relative content of elements. The atom ratio of Ca-Al-Cl in Friedel’s salt ($3\text{CaO}\cdot\text{Al}_2\text{O}_3\cdot\text{CaCl}_2\cdot 10\text{H}_2\text{O}$) is 4:2:2, while the atom ratio of Ca-Al-S in AFt ($3\text{CaO}\cdot\text{Al}_2\text{O}_3\cdot\text{CaSO}_4\cdot 12\text{H}_2\text{O}$) is 4:2:1. Table 5 shows that dot 1 represents Kuzel’s salt ($3\text{CaO}\cdot\text{Al}_2\text{O}_3\cdot 0.5\text{CaCl}_2\cdot 0.5\text{CaSO}_4\cdot 12\text{H}_2\text{O}$) with a Ca-Al-S-Cl ratio of 4.2:2:1.1:0.57; dot 2 mainly consists of Friedel’s salt with a Ca-Al-S-Cl ratio of 4.4:2:0:1.8. Since a mixture of 2/3 AFt and 1/3 Friedel’s salt was mixed, the Ca-Al-S-Cl ratio in dot 3 is 4:2:1:0 and 4.1:2:0:1.8, and dot 4 has ratios of 4:2:1:0 and 3.6:2:0:1.5, respectively. The concentration of calcium is slightly higher due to the effects of zeolite minerals and unreacted $\text{Ca}(\text{OH})_2$. Overall, there were AFt, Friedel’s salt, and Kuzel’s salt generated in the geopolymer according to the XRD, SEM, and EDS results.

Quantities of flake crystals can be seen in the OQ group in Figure 9a because $\text{Ca}(\text{OH})_2$ was generated when quicklime was combined with slag alone. The $\text{Ca}(\text{OH})_2$ content remaining in this group is still as high as 9.92% at 28 days, and the consumption of $\text{Ca}(\text{OH})_2$ is also lower, suggesting that the hydration degree is low when quicklime is employed alone and the enrichment of $\text{Ca}(\text{OH})_2$ crystals will also have a negative influence on the strength. Because gypsum interacts with C-A-H and produces a lot of AFt, quantities of acicular crystals may be visible in the LC group after adding 7.5% gypsum (as seen in Figure 9b LC \times 5000). Excessive AFt volume growth in the hardened paste may result in poor volume stability. Needle-rod and flake crystals are readily visible in Figure 9c LC \times 20,000. The reaction is completely dominated by NaCl, yielding coarse needle-rod

Friedel's salt and flake Kuzel's salt. The XRD pattern also shows that the diffraction peak intensity of Friedel's salt in the LC group was lower than that of L0, indicating that the concentration of Friedel's salt declines, while the amount of Kuzel's salt grows.

NaCl functions as an auxiliary activator in the hydration reaction, releasing the alkali metal cation Na^+ and generating NaOH; NaOH offers an alkaline environment for slag hydration [41]. The hydration of slag in an alkaline environment experienced the dissolution and diffusion of aluminosilicate minerals in alkaline solution, the polymerization of aluminosilicate solutions and complexes caused by the gel phase ($\text{M}_x(\text{AlO}_2)_y(\text{SiO}_2)_z \cdot n\text{MOH} \cdot m\text{H}_2\text{O}$), and the consolidation and hardening process of the gel phase [42], in which the polymerization refers to the chemical reaction between various aluminosilicates and strong alkaline silicate solutions [43,44]. In addition to the aforementioned process, activated silicon oxide and activated alumina in slag react with $\text{Ca}(\text{OH})_2$ in an alkaline environment to form hydrated calcium silicate and hydrated calcium aluminate. Simultaneously, sodium hydroxide can generate a geopolymer by reacting with active silica and active alumina [45]. In addition, slag can also reduce the diffusion rate of Cl^- [46] and produce Friedel's salt. One of the AFm compounds is Friedel's salt. There are several different forms of AFm compounds, and their chemical makeup varies widely. The majority of them are lamellar crystals, with the most common being $3\text{CaO} \cdot \text{Al}_2\text{O}_3 \cdot \text{CaSO}_4 \cdot x\text{H}_2\text{O}$, $3\text{CaO} \cdot \text{Al}_2\text{O}_3 \cdot \text{CaCO}_3 \cdot x\text{H}_2\text{O}$, and $3\text{CaO} \cdot \text{Al}_2\text{O}_3 \cdot \text{CaCl}_2 \cdot x\text{H}_2\text{O}$ [47,48]. Because the addition of NaCl and gypsum causes Cl^- , SO_4^{2-} , CO_3^{2-} , and other ions to exist in the hydration reaction, it may simultaneously produce a variety of compounds, such as hydrated calcium chloroaluminate, hydrated calcium sulphoaluminate, hydrated calcium carboaluminate, and more complex compounds produced after the substitution of each acid radical ion. The hydration products containing Cl^- are $3\text{CaO} \bullet \text{Al}_2\text{O}_3 \bullet \text{CaCl}_2 \bullet x\text{H}_2\text{O}$, C-S-H gels, and zeolite containing SO_4^{2-} , Mg^{2+} , and Na^+ . The molecular formula of the lamellar crystal and needle-rod crystal components is $3\text{CaO} \cdot \text{Al}_2\text{O}_3 \cdot (0.5\text{CaCl}_2 \cdot 0.5\text{CaSO}_4) \cdot 12\text{H}_2\text{O}$, which is extremely close to the insoluble Kuzel's salt.

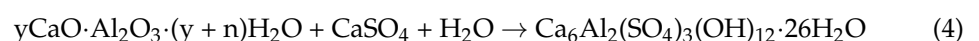
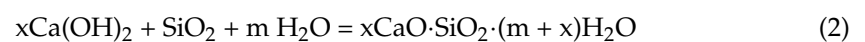
It has been established that NaCl participates in the hydration process and generates chlorine-containing molecules. The released Na^+ generates NaOH, which raises the PH of the geopolymer and promotes the hydration of slag, hence increasing strength. The addition of NaCl can promote the dissolution of gypsum, thus accelerating SO_4^{2-} to form AFt [30,49], providing early strength and compensating for shrinkage. AFt is produced before Friedel's salt when NaCl is added. With the extension of hydration age, NaCl is easier to react with C-A-H and AFt to produce Friedel's salt [22]. Meanwhile, chloride and sulfate react with C-A-H and AFt to form Kuzel's salt [50–53]; the creation of Friedel's salt and Kuzel's salt consumes Cl^- , and the released OH^- combines with Na^+ to generate NaOH, enhancing the alkalinity and accelerating slag hydration. Simultaneously, the creation of Kuzel's salt consumes SO_4^{2-} and decreases the quantity of AFt in the hardened paste.

The hydration reaction equation of the slag-based geopolymer activated by NaCl, gypsum, and quicklime are as follows:

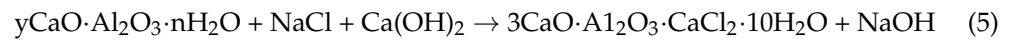
(1) CaO in the compound activator reacts with water:



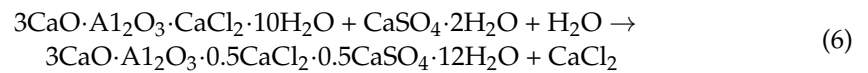
(2) In an alkaline environment, OH^- depolymerizes Ca-O, Si-O, and Al-O bonds in the vitreous body and accelerates the slag reaction, which results in hydration products such as C-S-H gel and calcium aluminate hydrate [54–56]:



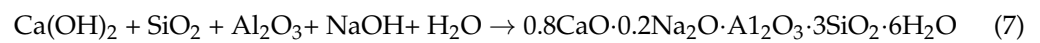
(3) In addition to AFt, partially hydrated calcium aluminate ($y\text{CaO}\cdot\text{Al}_2\text{O}_3\cdot(y+n)\text{H}_2\text{O}$) reacted with $\text{Ca}(\text{OH})_2$ and NaCl to form Friedel's salt and NaOH:



(4) The addition of gypsum provided SO_4^{2-} , and part of Friedel's salt continued to react with gypsum, replacing part of the Cl^- and generating Kuzel's salt ($3\text{CaO}\cdot\text{Al}_2\text{O}_3\cdot 0.5\text{CaCl}_2\cdot 0.5\text{CaSO}_4\cdot 12\text{H}_2\text{O}$) [37]:



(5) The NaOH generated in reaction (5) can be employed as an activator in the formation of zeolite ($0.8\text{CaO}\cdot 0.2\text{Na}_2\text{O}\cdot\text{Al}_2\text{O}_3\cdot 3\text{SiO}_2\cdot 6\text{H}_2\text{O}$) by reacting with slag:



The hydration reaction mechanism in the cementitious system is shown in Figure 11. And the reaction Equations (1)–(7) are labeled.

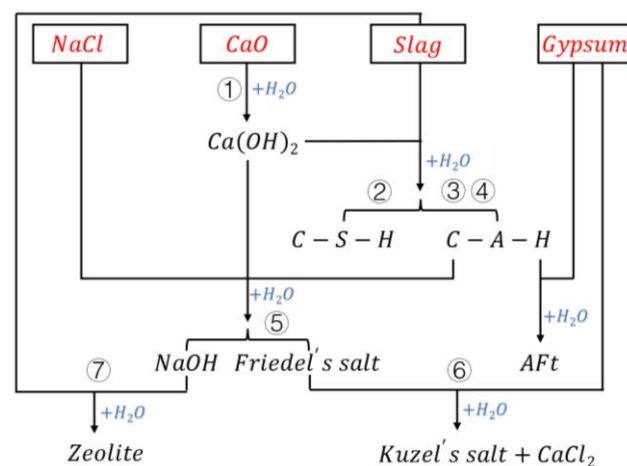


Figure 11. Hydration reaction diagram.

3.1.4. MIP

Based on the study of the hydration mechanism and product composition of the slag-based geopolymer, the pore structure of hardened paste was analyzed using MIP.

According to Figure 12, the most likely pore size of the LC group is 30 nm, and the pore size distribution curve is largely below that of the OC group in the 10 to 100 nm range, indicating that the pore volume of the LC group is smaller than that of the OC group. This is due to the crystals of Friedel's salt and Kuzel's salt filling the pores between gels and increasing the density of hardened paste. At 28 days, the CCW-NCH content of the LC group is greater than that of the OC, L0, and OQ groups. NaCl and gypsum boosts slag hydration and the formation of additional gel phases, which raises the compactness of hardened paste and decreased porosity. Pores in the OC group are spread in the 100–130 nm range, but those in the LC group vanish, and the pore size distribution curve of the LC group between 50,000 and 400,000 nm was much smaller than those of the OC, L0, and OQ groups. The damaging pores cause a decrease in strength. As a result, the LC group has fewer damaging pores and greater strength. The L0 group has the most pores in the 10–30 nm and 20,000–40,000 nm ranges, and its porosity is the highest among the four groups.

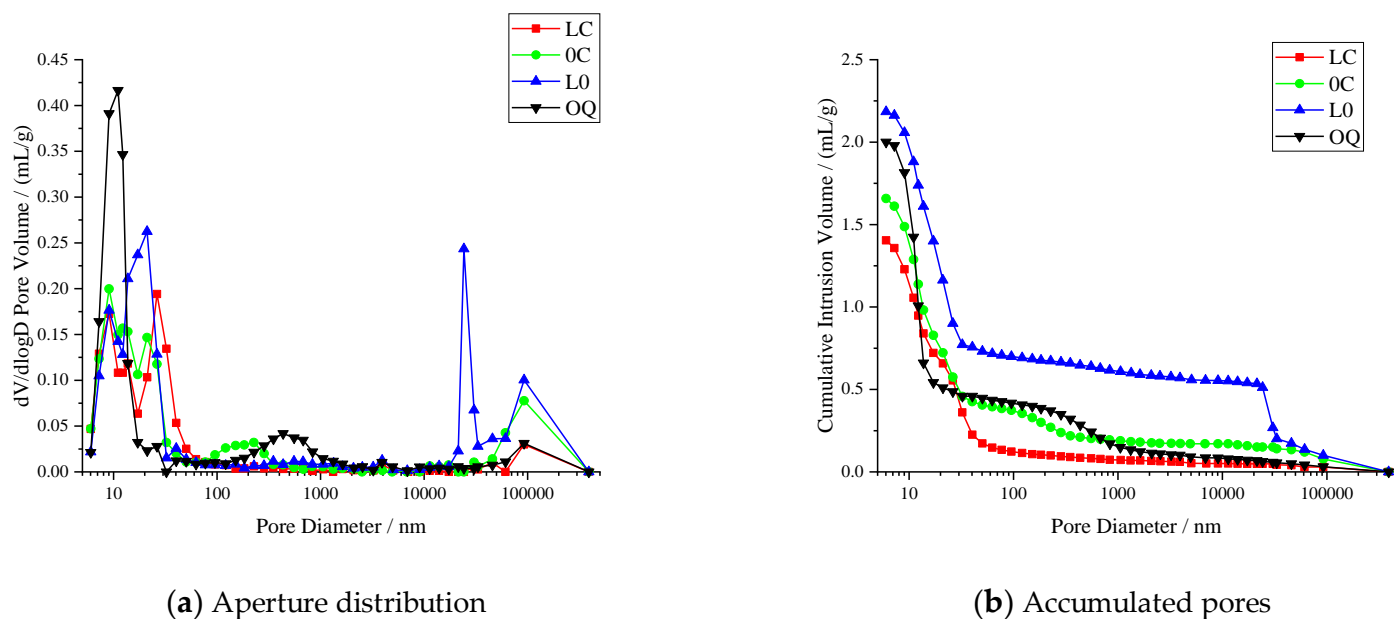


Figure 12. Pore structure analysis curve of different mixture proportions.

The D value of pore fractal dimension describes the pore section's complexity. The more intricate the spatial distribution of the pores, the higher the score. The greater the fractal dimension of pore volume, the more complex the spatial geometric properties of pores can be interpreted from fractal theory and pore fractal model, i.e., the more complicated the spatial distribution of pores in the material and the stronger the spatial filling ability. It also implies that when the pores are reduced, the average pore size lowers, the number of macropores reduces, the number of tiny holes grows, and the specific surface area of the pores increases, implying that the pore structure is refined and optimized to some extent. Therefore, the fractal dimension of pore volume may be regarded as an all-encompassing characteristic of pore form and spatial distribution [57]. As shown in Figure 13, using NaCl and quicklime (L0) as activators enhanced porosity by 46.7% when compared to quicklime alone. Porosity rose by 9.9% when gypsum and lime (OC) were employed as activators instead of quicklime alone. The porosity was reduced by 18.7% when NaCl, gypsum, and quicklime (LC) were employed simultaneously. The fractal dimension shrunk from 2.9 to 2.0. Porosity rose with single additions of NaCl or gypsum but decreased with compound additions of NaCl and gypsum.

XRD results show that there are no Friedel's salt and Kuzel's salt diffraction peaks in the OC group, and no Friedel's salt and Kuzel's salt crystals are found in SEM photos. Friedel's salt and Kuzel's salt could not be produced without NaCl or gypsum, and they could not play the role of filling pores, so the porosity of the OC group is higher. Crystal products cross-link in the pores and compact the paste [58], which is beneficial to the strength and volume stability. Friedel's salt and Kuzel's salt diffraction peaks were not discovered in the OC group, and no Friedel's salt and Kuzel's salt crystals were found in SEM pictures. Friedel's salt and Kuzel's salt cannot be made without NaCl or gypsum, and they cannot fill pores; therefore, the porosity of the OC group is larger. Crystal products form cross-links in the pores and compact the paste, which can improve strength and volume stability.

3.2. Strength of Mortar

The compressive strength of geopolymer mortar at 3 days and 28 days is shown in Figure 14.

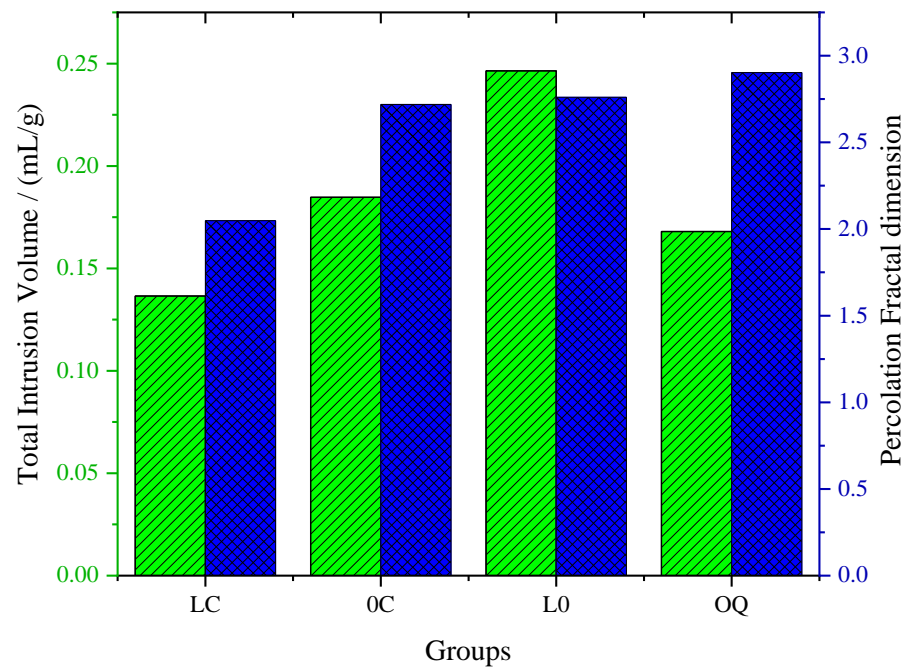


Figure 13. Porosity and fractal dimension.

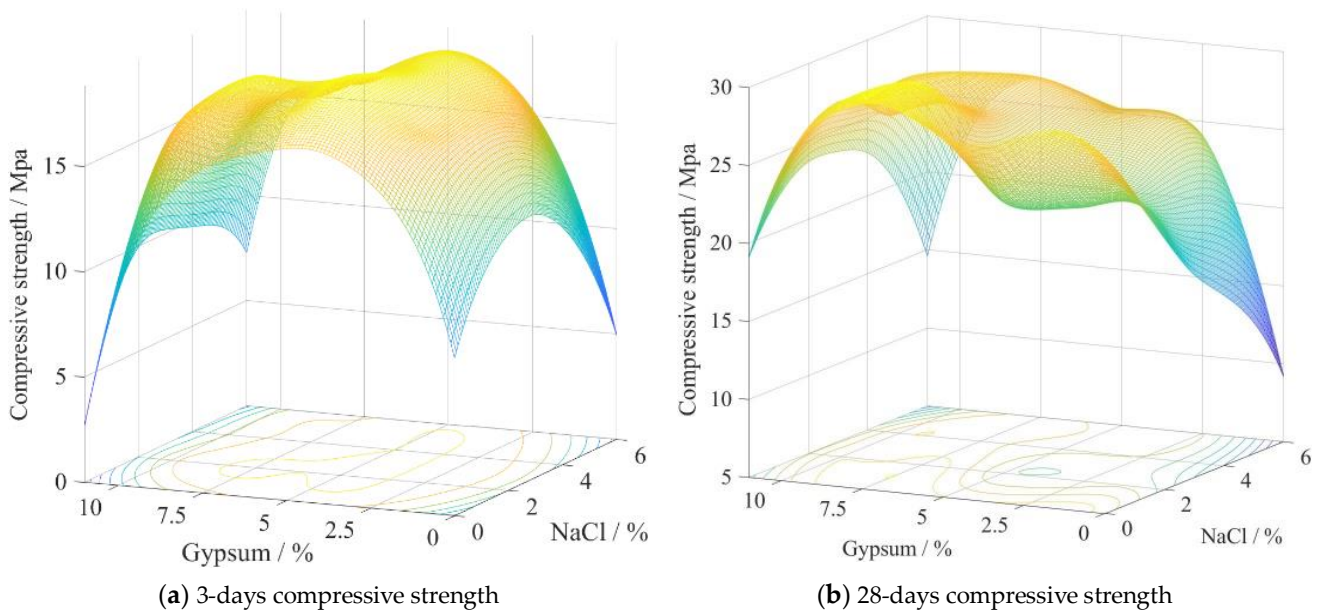


Figure 14. Fitting surface of compressive strength of mortar.

According to Figure 14a, the inclusion of a combination of 2% NaCl and 5% gypsum can significantly enhance the 3-day strength of the material, and the maximum 3-day compressive strength achieved is 18.8 MPa. Specifically, when the NaCl dosage is maintained at 2%, the 3-day compressive strength initially experiences a gradual increase as the amount of gypsum is increased from 0 to 5%, but then undergoes a sharp decline upon further increase in the gypsum content from 7.5% to 10%. Furthermore, the addition of 7.5% gypsum leads to a noteworthy increase of 48.8% in the 3-day strength, from an initial value of 12.5 MPa to 18.6 MPa. However, the strength subsequently declines as the gypsum content is increased to 10%. The 3-day compressive strength exhibits a 25.6% increase from 14.8 MPa to 18.6 MPa as NaCl increases from 0 to 2% when the gypsum content is 7.5%; however, the strength decreases by 15.1% when the NaCl content is further increased from 2 to 6%.

Based on Figure 14b, incorporating a mixture of 2% NaCl and 7.5% gypsum can enhance the 28-day compressive strength of the material. Specifically, when the gypsum content is 7.5%, the 28-day compressive strength initially experiences a slight improvement as the NaCl content increases from 0 to 2%, but then undergoes a decline when the NaCl content is increased from 4 to 6%. When the gypsum content is 10%, the 28-day compressive strength decreases monotonically with an increase in NaCl content. Moreover, when the NaCl content is maintained at 2%, the 28-day compressive strength initially increases gradually as the gypsum content is increased from 0 to 7.5%, but then experiences a decline as the gypsum content is further increased from 7.5 to 10%. Significantly, the addition of 7.5% gypsum results in a notable 63.8% increase in the 28-day compressive strength, from an initial value of 18.0 MPa to 29.5 MPa, which represents the maximum value achieved.

The LC with a 25% activator displayed the highest strength when compared to LC with 20%, 30%, and 35% activators. The optimal activating effect is achieved by utilizing a mixture of NaCl, gypsum, quicklime, and slag in the proportions of 2:7.5:15.5:75 (LC), which resulted in a 148% increase in 3-day compressive strength and a 37.85% increase in 28-day compressive strength, as compared to the OQ group. The 28-day rupture strength of the LC group is found to be 9.9 MPa; additionally, the 28-day compressive strength of the LC group reached 29.5 MPa, and the compressive strength at 56 days reached 34.2 MPa.

The addition of gypsum has a significant impact on the strength of the geopolymer. A low gypsum dosage (2.5%) results in insufficient sulfate content, which limits the activation of the slag. Conversely, a high gypsum dosage (10%) decreases the quicklime content, which is necessary for the hydration reaction of the slag. Additionally, excessive gypsum continues to react in the hardened paste and generate Aft, causing volume expansion that may damage the hardened paste structure. At a 7.5% gypsum dosage, adding 2% NaCl can significantly improve 3-day compressive strength; however, further increases in NaCl content can result in decreased strength.

The experimental results demonstrate that the geopolymer achieves its highest strength when quicklime content is approximately 15.5%, mainly because the CaO is the source of $\text{Ca}(\text{OH})_2$ in the system. Insufficient quicklime content leads to a depletion of $\text{Ca}(\text{OH})_2$ content in the geopolymer, resulting in incomplete reactions of slag and inadequate hydration products that are unable to form an effective space network structure in the geopolymer. Sufficient quicklime content can result in a high pH value, creating a highly alkaline environment, promoting the disintegration of the slag, releasing active components such as silica tetrahedrons and alumina tetrahedrons, accelerating the hydration process of slag, generating more C-S-H, and enhancing the density of the geopolymer. However, excessive amounts of quicklime not only reduce the proportion of slag in the geopolymer, but the excess Ca^{2+} and OH^- causes the formation of hexagonal flake $\text{Ca}(\text{OH})_2$ crystals, which have poorer microscopic properties than other hydration products, such as C-S-H, resulting in lower strength.

When slag is activated by quicklime alone, its hydration degree is limited. As a result, the OQ group has the lowest CCW-NCH content and a 3-day compressive strength of only 7.5 MPa, despite having a $\text{Ca}(\text{OH})_2$ content of 10.95% after 3 days. After adding 2% NaCl and 7.5 gypsum, compared to the OQ group, CCW-NCH content at 3 and 28 days increased by 4.64% and 5.07%. This results in an increase in compressive strength of 148% and 37.85% at 3 days and 28 days, respectively.

The LC group achieved the highest 28-d compressive strength. In this group, the combination of NaCl and gypsum leads to the generation of NaOH through the interaction with C-A-H, thereby promoting slag hydration and increasing its strength. Gypsum can stimulate slag activity and enhance its hydration, leading to increased strength. However, excessive amounts of gypsum can lead to the production of excessive amounts of Aft [59], resulting in volume expansion and the breaking of hardened paste. Previous studies have shown that the optimal proportion of gypsum in slag-based geopolymer is between 6% and 10% [60]. Additionally, the reactivity of slag powder increases significantly when the concentration of gypsum and quicklime is within the range of 5–10% and 10–20%,

respectively [61]. The appropriate dosage of gypsum and sodium chloride in this study is consistent with these findings.

The LC group exhibits higher rupture strength due to the formation of more crystalline materials such as AFt and Kuzel's salt. The AFt content is as high as 12.61%, which improves the compactness of the paste by filling the pores and increases rupture strength by withstanding tensile stress better than the gel phase. The LC group achieved the highest 28-day compressive strength of 29.5 MPa due to the gradual depolymerization of the vitreous network structure in slag resulting from the synergistic activation of quicklime and gypsum. AFt and C-S-H gel are the primary hydration products in the early stage of hardened paste. As the hydration process continues, crystal products pack into the paste's pores and are tightly bonded to the whole, enhancing the compactness of the paste structure and improving early mortar strength [62]. C-A-H interacts with Cl^- and SO_4^{2-} to form Friedel's salt and Kuzel's salt as it ages. The addition of NaCl and gypsum provides Cl^- and SO_4^{2-} for the creation of Kuzel's salt. Kuzel's salt is an insoluble salt that fills the paste's pores and contributes to strength, while the development of zeolite minerals also improves strength.

3.3. Soundness, Crack Resistance, and Shrinkage

Visible cracks in the geopolymer paste are shown in Figure 15.

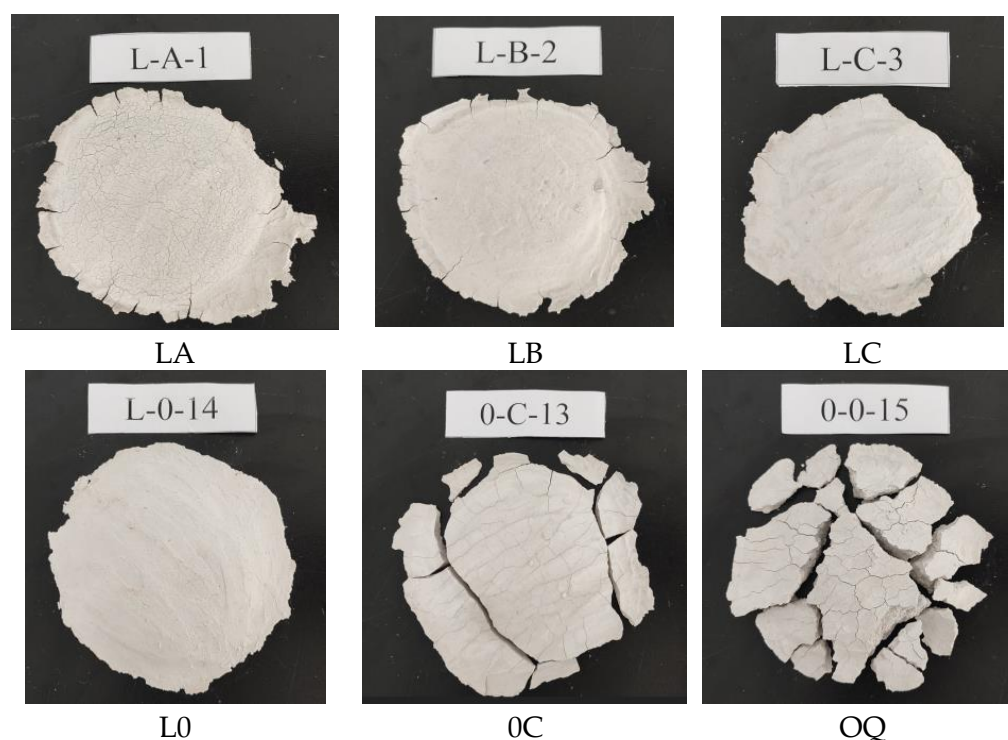


Figure 15. Cracking test of geopolymer paste.

As shown in Figure 15, gypsum has a positive effect on the stability of slag geopolymers. The LA group exhibits numerous micro-cracks on the surface, accompanied by multiple piercing fractures along the edge. As the amount of gypsum increases, the LB group exhibits fewer surface fissures and no visible fractures, while the LC group shows no discernible cracks. Furthermore, gypsum also leads to an improvement in the 28-day compressive strength. Appropriate NaCl content also confers a significant advantage in enhancing stability. During the hardening process, the OQ group experiences severe cracking within an hour, resulting in fractured surfaces broken into small pieces. X-ray diffraction (XRD) patterns show significant peaks for $\text{Ca}(\text{OH})_2$, thermogravimetric (TG) analysis indicates that over 60% of $\text{Ca}(\text{OH})_2$ remains unreacted with slag after three days,

and scanning electron microscopy (SEM) reveals the presence of many hexagonal flake $\text{Ca}(\text{OH})_2$ crystals. In contrast, the L0 group treated with 2% NaCl does not exhibit any cracks. The addition of NaCl and gypsum to the LC group almost completely eliminates the cracks. Both NaCl and gypsum enhance the stability of slag-based geopolymers, with NaCl having the most significant impact.

According to Figure 16a, the 14-day autogenous shrinkage of the LC group is 0.48×10^{-3} , which is similar to the OPC group's autogenous shrinkage of 0.45×10^{-3} . In addition, as seen in Figure 16b, the early drying shrinkage growth trend of the LC group is similar to that of the OPC group, but the LC group begins to gradually stabilize at 7 days, whereas the OPC group begins to gradually stabilize at 21 days. The drying shrinkage of the LC group at 28 days is just 0.48×10^{-3} , which is only 66.7% of OPC. The addition of gypsum supplies SO_4^{2-} to form Aft in the hydration products, leading to volume expansion and compensating for shrinkage [63]. MIP results indicate that the porosity of the LC group is low, as the crystal products of Friedel's salt and Kuzel's salt fill the pores, resulting in the lowest porosity of the LC group. Consequently, the capillary pore negative pressure is low, and the autogenous shrinkage is also small.

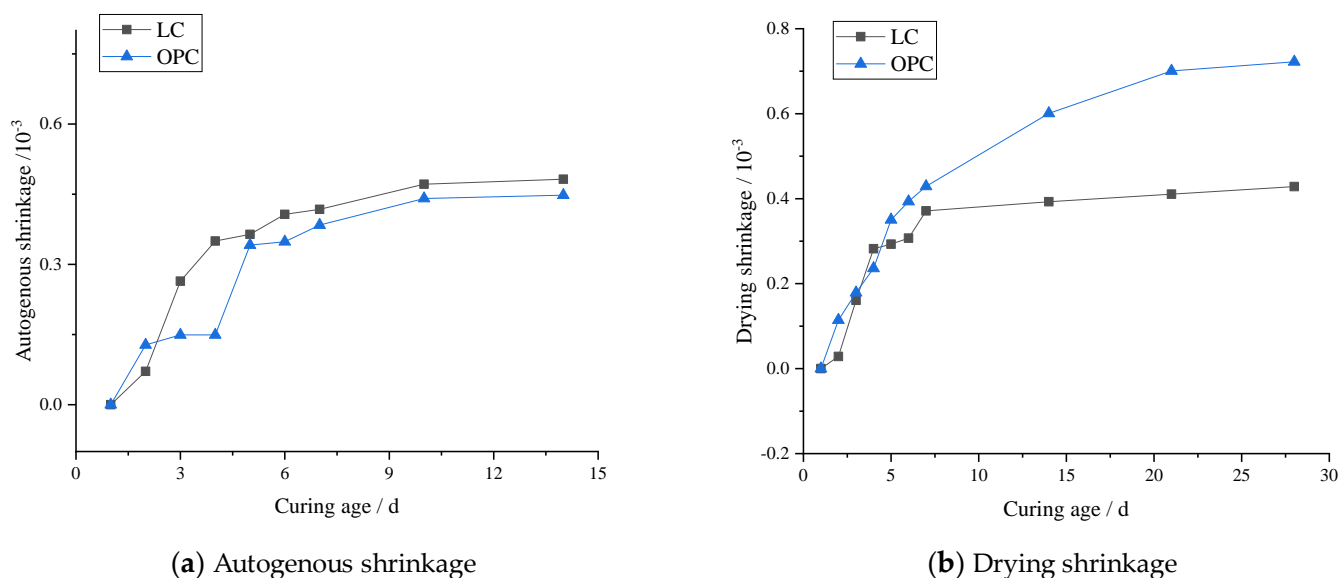


Figure 16. Shrinkage comparison.

Both drying shrinkage and autogenous shrinkage are caused by a decrease in water in the pores of hardened cement paste, resulting in certain pores being unable to be saturated by water. The hydrophilic capillary wall causes the water surface in the pores to form a meniscus, which brings the particles around the pores closer together, resulting in a reduction of the paste's macro volume [64,65]. The gel has a more porous structure in concrete, making it more prone to shrinkage and cracking, whereas the total drying shrinkage strain of typical slag-based geopolymers can reach as high as $1700 \mu\epsilon$ [66,67], which is four times that of ordinary concrete [68,69]. The drying shrinkage of slag-based geopolymers activated by sodium hydroxide and water glass is much greater than that of Portland cement [70,71]. According to Cartwright's research, the shrinkage value of slag-based geopolymer is six times more than that of Portland cement [19]. Atis et al. compares the drying shrinkage of slag-based geopolymers to the impacts of liquid sodium silicate, sodium hydroxide, and sodium carbonate, and determined that the shrinkage of slag-based geopolymer activated by liquid sodium silicate and sodium hydroxide is greater [20]. When sodium hydroxide or sodium silicate is employed as an activator, the drying shrinkage can be three to six times that of Portland cement mortar [18], which is a major cause for the failure of slag-based geopolymer applications on a wide scale. However,

slag-based geopolymers activated by NaCl, gypsum, and quicklime exhibit lower shrinkage than the OPC group and demonstrate a promising potential for broad application.

As shown in Figure 17, all test groups did not crack in 28 days, showing good crack resistance, the same as the OPC group. The addition of NaCl and gypsum, as well as their combination, does no harm to the crack resistance of the geopolymer. According to research, slag-based geopolymer mortar activated by sodium silicate and sodium hydroxide breaks along the radial direction in the ring cracking test, and the frequency of cracks near the limit column rises [72]; this is due to the substantial shrinkage of slag-based geopolymer activated by sodium silicate, which causes stress concentration at the limiting prism angle, resulting in cracking. Differently, the volume expansion of Aft compensates for shrinkage, and the volume stress induced by lesser volume shrinkage is smaller; therefore, the compound geopolymer does not crack. Obviously, when compared to the slag-based geopolymer activated by water glass and caustic soda, the slag-based geopolymer activated by NaCl, gypsum, and quicklime has better stability, shrinkage, and fracture resistance, which is important for engineering applications.

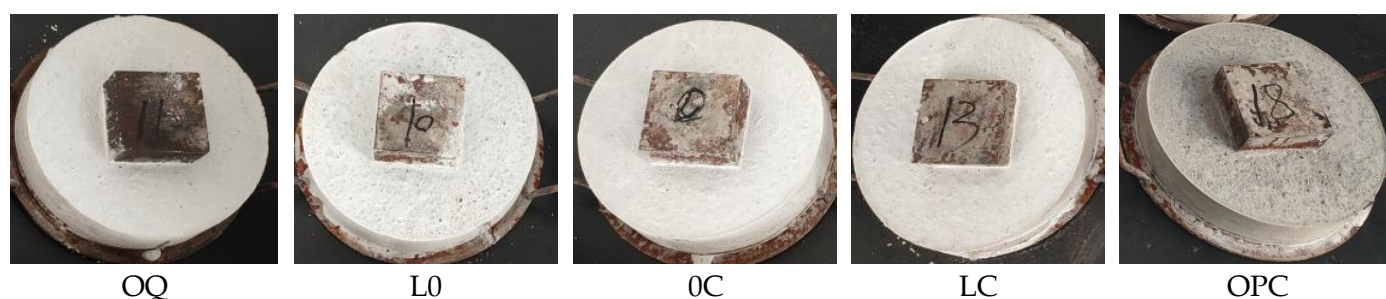


Figure 17. Square circle anti-cracking test of the geopolymer.

4. Conclusions

In this study, the mechanical properties and hydration mechanism of slag-based geopolymer activated by sodium chloride, gypsum, and quicklime were investigated. The following conclusions can be drawn based on the results presented:

(1) Needle-like crystal Aft, Friedel's salt, and flake Kuzel's salt are generated in the slag-based geopolymer activated by NaCl compounding gypsum. Na⁺ is released when Friedel's salt is formed, thus promoting the hydration of slag. Under the combined effect of NaCl and gypsum, the amount of Aft as well as Ca(OH)₂ is decreased, while the chemical combined water is increased by 4.64% and 5.07% at 3 days and 28 days. In addition, the porosity is reduced by 18.7% for the filling effect of those crystal products.

(2) There is a superimposed effect on compressive strength when 2% NaCl and 7.5% gypsum are combined. By using a NaCl: gypsum: quicklime: slag ratio of 2:7.5:15.5:75 (the LC group), the compressive strengths were increased by 148% and 37.8%, respectively, compared to the 00 group. The LC's compressive strength at 3 days, 28 days, and 56 days were 18.6 MPa, 29.5 MPa, and 34.2 MPa, respectively. Under appropriate dosage, the formation of Aft, Friedel's salt, and Kuzel's salt through the addition of NaCl and gypsum is beneficial for enhancing the strength of the geopolymer. The combined employment of both sodium chloride and gypsum effectively addresses the issue of 28-day strength reduction that arises when sodium chloride is used in isolation and the problem of poor paste soundness that arises when gypsum is used alone.

(3) According to the square circle anti-crack tests, the co-presence of NaCl and gypsum in the slag-based geopolymer does not have a detrimental effect on crack resistance. In addition, the autogenous shrinkage of the LC group was found to be similar to the OPC group, and the drying shrinkage was only 66.75% of that of the OPC group. Generally, the shrinkage of slag-based geopolymer activated by strong alkali can reach several times that of ordinary Portland cement, so the shrinkage of the slag-based geopolymer activated by the composite activator is much smaller than that of the geopolymer activated by strong alkali.

(4) This geopolymer is made from cheap and easily available industrial products, such as sodium chloride, gypsum, quicklime, and slag, and does not use strong alkali activators; therefore, this geopolymer is more economical and energy-efficient and has lower carbon emissions than geopolymers activated by strong alkali, rendering it an environmentally friendly and cost-effective cementitious material in plain concrete applications. More research, such as frost resistance, carbonization resistance, etc., will be conducted in the future. The application of this geopolymer to solidify coastal saline soils is also ongoing.

Author Contributions: Conceptualization, W.H. and X.M.; methodology, W.H. and Q.S.; validation, W.H. and Q.S.; formal analysis, B.L. and Q.S.; investigation, B.L. and Q.S.; data curation, Y.S. and Q.S.; writing—original draft preparation, B.L. and X.M.; funding acquisition, W.H. and Y.S. All authors have read and agreed to the published version of the manuscript.

Funding: This work is sponsored by the National Key R&D Program of China (2022YFC3803400), National Natural Science Foundation of China (No. 52208413 and 52008011), Beijing Municipal Natural Science Foundation (No. 8204058), BUCEA Post Graduate Innovation Project (No. 02081022003), and the R&D Program of Beijing Municipal Education Commission (No. KM202210016011).

Data Availability Statement: The data used to support the findings of this study are available from the corresponding author upon request.

Conflicts of Interest: The authors declare no conflict of interest.

References

- Jesus, C.F.; Arruda Junior, E.S.; Braga, N.T.S.; Silva Junior, J.A.; Barata, M.S. Coloured concrete produced from low-carbon cements: Mechanical properties, chromatic stability and sustainability. *J. Build. Eng.* **2023**, *67*, 106018. [[CrossRef](#)]
- Ijaz, N.; Ye, W.; Rehman, Z.U.; Ijaz, Z. Novel application of low carbon limestone calcined clay cement (LC3) in expansive soil stabilization: An eco-efficient approach. *J. Clean. Prod.* **2022**, *371*, 133492. [[CrossRef](#)]
- Yang, T.; He, X. Research status and prospect of blast furnace slag resource utilization. *China Environ. Prot. Ind.* **2020**, *3*, 4.
- Ahmadi, H.; Khalaj, G.; Najafi, A.; Abbasi, S.M.; Safari, M. Metakaolin-red mud/carbon nanotubes geopolymer nanocomposite: Mechanical properties and structural studies. *Mater. Res. Express* **2022**, *9*, 025011. [[CrossRef](#)]
- Salami, B.A.; Ibrahim, M.; Al-Osta, M.A.; Nasir, M.; Ali, M.R.; Bahraq, A.A.; Wasu, A. Engineered and green natural pozzolan-nano silica-based alkali-activated concrete: Shrinkage characteristics and life cycle assessment. *Environ. Sci. Pollut. Res.* **2023**, *30*, 17840–17853. [[CrossRef](#)]
- Cui, K.; Liang, K.; Chang, J.; Lau, D. Investigation of the macro performance, mechanism, and durability of multiscale steel fiber reinforced low-carbon ecological UHPC. *Constr. Build. Mater.* **2022**, *327*, 126921. [[CrossRef](#)]
- Provis, J.L.; Bernal, S.A. Geopolymers and Related Alkali-Activated Materials. *Annu. Rev. Mater. Res.* **2014**, *44*, 299–327. [[CrossRef](#)]
- Nasir, M.; Johari, M.A.M.; Maslehuddin, M.; Yusuf, M.O. Sodium sulfate resistance of alkali/slag activated silico-manganese fume-based composites. *Struct. Concr.* **2021**, *22* (Suppl. S1), E415–E429. [[CrossRef](#)]
- Sofi, M.; Deventer, J.S.J.V.; Mendis, P.A.; Lukey, G.C. Engineering properties of inorganic polymer concretes (IPCs). *Cem. Concr. Res.* **2007**, *37*, 251–257. [[CrossRef](#)]
- Rashad, A.M.; Zeedan, S.R.; Hassan, A.A. Influence of the activator concentration of sodium silicate on the thermal properties of alkali-activated slag pastes. *Constr. Build. Mater.* **2016**, *102*, 811–820. [[CrossRef](#)]
- Bakharev, T. Resistance of geopolymer materials to acid attack. *Cem. Concr. Res.* **2005**, *35*, 658–670. [[CrossRef](#)]
- Bakharev, T. Durability of geopolymer materials in sodium and magnesium sulfate solutions. *Cem. Concr. Res.* **2005**, *35*, 1233–1246. [[CrossRef](#)]
- Yang, N.R. Physicochemical basis of formation of alkali cementitious materials. *J. Chin. Ceram. Soc.* **1996**, *24*, 209–215. [[CrossRef](#)]
- Roy, D.M. Alkali-activated cements Opportunities and challenges. *Cem. Concr. Res.* **1999**, *29*, 249–254. [[CrossRef](#)]
- Shi, C.J. Strength, pore structure and permeability of alkali-activated slag mortars. *Cem. Concr. Res.* **1996**, *26*, 1789–1799. [[CrossRef](#)]
- Fu, Y.W.; Cai, L.C.; Wu, Y.J. Freeze-thaw cycle test and damage mechanics models of alkali-activated slag concrete. *Constr. Build. Mater.* **2011**, *25*, 3144–3148. [[CrossRef](#)]
- Fu, Y.W.; Cai, L.C.; Cao, D.G.; Wu, Y.G. Freeze-thaw durability and damage mechanics model of high performance alkali-slag concrete. *Eng. Mech.* **2012**, *23*, 103–109.
- Duxson, P.; Provis, J.L.; Lukey, G.C.; Deventer, J.S.J.V. The role of inorganic polymer technology in the development of 'green concrete'. *Cem. Concr. Res.* **2007**, *37*, 1590–1597. [[CrossRef](#)]
- Collins, F.; Sanjayan, J.G. Strength and Shrinkage Properties of Alkali-Activated Slag Concrete Containing Porous Coarse Aggregate. *Cem. Concr. Res.* **1999**, *29*, 607–610. [[CrossRef](#)]
- Zhang, L.F. *Alkali Activated Slag Cement and Concrete*, 1st ed.; Southwest Jiaotong University Press: Chengdu, China, 2018; pp. 132–140. ISBN 978-7-5643-6401-4.

21. Cartwright, C.; Rajabipour, F.; Radlinska, A. Shrinkage Characteristics of Alkali-Activated Slag Cements. *J. Mater. Civ. Eng.* **2014**, *27*, B4014007. [[CrossRef](#)]
22. Atiş, C.D.; Bilim, C.; Çelik, Ö.; Karahan, O. Influence of activator on the strength and drying shrinkage of alkali-activated slag mortar. *Constr. Build. Mater.* **2009**, *23*, 548–555. [[CrossRef](#)]
23. Ibrahim, M.; Nasir, M.; Hussaini, S.R.; Najamuddin, S.K.; Ewebajo, A. Performance of structurally viable green concrete derived from natural pozzolan and nanosilica. *Mag. Civ. Eng.* **2021**, *7*, 10710.
24. Cheng, Y.; Huang, X. Effect of chloride on strength of alkali activated slag paste. *J. Beijing Univ. Aeronaut. Astronaut.* **2015**, *4*, 693–700. [[CrossRef](#)]
25. Lv, Q.F.; Wang, Z.S.; Cheng, Y. Effect mechanism of sodium chloride on strength of alkali-activated geopolymer. *J. Funct. Mater./Gongneng Cailiao* **2020**, *51*, 73–98+7. [[CrossRef](#)]
26. Cao, Y.Z.; Guo, L.P.; Xue, X.L. Effects of sodium chloride and sodium sulfate on hydration process. *J. Southeast Univ. (Nat. Sci. Ed.)* **2019**, *49*, 8. [[CrossRef](#)]
27. He, W. Effects of sodium chloride on the mechanical properties of slag composite matrix geopolymer. *Adv. Cem. Res.* **2019**, *31*, 389–398. [[CrossRef](#)]
28. Liu, C.B.; Gao, X.Q.; Zhou, Y.C. Research on hydration mechanism of slag composite cementitious material mixed with NaCl. *J. Chem. Pharm. Res.* **2014**, *6*, 845–849.
29. Zhang, L.F.; Song, S.S.; Liang, Q.S. Effect of gypsum content on properties of alkali-activated slag cement mortar. *Appl. Chem. Ind.* **2020**, *49*, 6. [[CrossRef](#)]
30. Xing, J.; Hu, J.W.; Li, C.; Qiu, J.P.; Sun, X.G. The effect of gypsum on the cementitious performance of blast furnace slag stimulated by calcium oxide. *China Min. Mag.* **2019**, *28*, 166–171. [[CrossRef](#)]
31. Provis, J.L.; Lukey, G.C.; Deventer, J.V. Do Geopolymers Actually Contain Nanocrystalline Zeolites? A Reexamination of Existing Results. *Chem. Mater.* **2005**, *17*, 3075–3085. [[CrossRef](#)]
32. Zhang, Y.X.; Yang, Z.H.; Guo, D.; Geng, H.; Dong, C. Effect of chloride salts and bicarbonate on solubility of CaSO₄ in aqueous solutions at 37 °C. *Procedia Environ. Sci.* **2013**, *18*, P84–P91. [[CrossRef](#)]
33. Liu, C.B.; Yuan, Y.K.; He, W.; Zhang, L. Durability analysis of seashore saline soil bound with a slag compound binder. *Soils Found.* **2019**, *59*, 1456–1467. [[CrossRef](#)]
34. Xiong, L.C.; Wan, Z.J.; Zhang, Y.; Wang, F.T.; Kang, Y.L. Fly ash particle size effect on pore structure and strength of fly ash foamed geopolymer. *Adv. Polym. Technol.* **2019**, *2019*, 1098027. [[CrossRef](#)]
35. Carlson, R.W.; Reading, T.J. Model Study of Shrinkage Cracking in Concrete Building Walls. *Struct. J.* **1988**, *85*, 395–404.
36. Luo, H.; Lv, L.Y.; Cui, H.Z. Research progress of cracking resistance evaluation methods for early age concrete. In Proceedings of the Industrial Architecture Academic Exchange Conference, Xi'an, China, 11–13 December 2020.
37. Song, S.M.; Shi, H.X.; Lian, H.Z.; Zhang, H.Y.; Zhang, L.Y. The utility model relates to a cracking sensitivity testing device for cement-based materials. U.S. Patent CN207198158U, 2018.
38. Ma, J.Y.; Li, Z.B. Preparation and desilication of Ca-Al hydrotalcite in sodium aluminate solution. *Sci. Sin. Chim.* **2010**, *40*, 577–584.
39. Mesbah, A.; François, M.; Cau-dit-Coumes, C.; Frizon, F.; Filinchuk, Y.; Leroux, F.; Ravaux, J.; Renaudin, G. Crystal structure of Kuzel's salt 3CaO·Al₂O₃·1/2CaSO₄·1/2CaCl₂·11H₂O determined by synchrotron powder diffraction. *Cem. Concr. Res.* **2011**, *41*, 504–509. [[CrossRef](#)]
40. Durdzinski, P.T. *Hydration of Multi-Component Cements Containing Cement Clinker, Slag, Calcareous Fly Ash and Limestone*; EPFL: Lausanne, Switzerland, 2016.
41. Ji, H.G.; Liu, C.B.; Liu, J.H. Characteristics of slag fine-powder composite cementitious material-cured coastal saline soil. *Emerg. Mater. Res.* **2014**, *3*, 282–291. [[CrossRef](#)]
42. Van Jaarsveld, J.; Van Deventer, J.; Schwartzman, A. The potential use of geopolymeric materials to immobilise toxic metals: Part II. Material and leaching characteristics. *Miner. Eng.* **1999**, *12*, 75–91. [[CrossRef](#)]
43. Jaarsveld, J.G.S.V.; Deventer, J.S.J.V.; Lukey, G.C. The characterisation of source materials in fly ash-based geopolymers. *Mater. Lett.* **2003**, *57*, 1272–1280. [[CrossRef](#)]
44. Xu, H.; Deventer, J.S.J.V. The geopolymerisation of alumino-silicate minerals. *International Journal of Mineral Processing. Int. J. Miner. Process.* **2000**, *59*, 247–266. [[CrossRef](#)]
45. Liu, C.B. The research of slag composite cementitious material strength and hydration mechanism. *Sichuan Build. Sci.* **2012**, *38*, 169–172. [[CrossRef](#)]
46. Roy, D.M.; Jiang, W.M.; Silsbee, M.R. Chloride diffusion in ordinary, blended, and alkali-activated cement pastes and its relation to other properties. *Cem. Concr. Res.* **2000**, *30*, 1879–1884. [[CrossRef](#)]
47. Matschei, T.; Lothenbach, B.; Glasser, F.P. The AFm phase in Portland cement. *Cem. Concr. Res.* **2007**, *37*, 118–130. [[CrossRef](#)]
48. Wang, S.D.; Huang, Y.B.; Wang, Z. Concrete resistance to chloride ingress: Effect of cement composition. *J. Chin. Ceram. Soc.* **2000**, *6*, 570–574. [[CrossRef](#)]
49. Haghtalab, A.; Badizad, M.H. Solubility of gypsum in aqueous NaCl + K₂SO₄ solution using calcium ion selective electrode-investigation of ionic interactions. *Fluid Phase Equilibria* **2016**, *409*, 341–353. [[CrossRef](#)]
50. Hirao, H.; Yamada, K.; Takahashi, H.; Zibara, H. Chloride Binding of Cement Estimated by Binding Isotherms of Hydrates. *J. Adv. Concr. Technol.* **2005**, *3*, 77–84. [[CrossRef](#)]

51. Ye, H.; Jin, X.Y.; Chen, W.; Fu, C.Q.; Jin, N.G. Prediction of chloride binding isotherms for blended cements. *Comput. Concr.* **2016**, *17*, 665–682. [[CrossRef](#)]
52. Birnin-Yauri, U.A.; Glasser, F.P. Friedel's salt, $\text{Ca}_2\text{Al}(\text{OH})_6(\text{Cl},\text{OH})\cdot 2\text{H}_2\text{O}$: Its solid solutions and their role in chloride binding. *Cem. Concr. Res.* **1998**, *28*, 1713–1723. [[CrossRef](#)]
53. Thomas, M.D.A.; Hooton, R.D.; Scott, A.; Zibara, H. The effect of supplementary cementitious materials on chloride binding in hardened cement paste. *Cem. Concr. Res.* **2012**, *42*, 1–7. [[CrossRef](#)]
54. Walther, J.V. Experimental determination of portlandite and brucite solubilities in supercritical H_2O . *Geochim. Et Cosmochim. Acta* **1986**, *50*, 733–739. [[CrossRef](#)]
55. Xing, G.F.; Xu, C.; Ye, G.B.; Yang, X.M. Mechanism Analysis of Influence of Soluble Salt Ions on Strength of Salt-rich Cement-soil. *China J. Highw. Transp.* **2008**, *21*, 26–30. [[CrossRef](#)]
56. Yi, Y.L.; Liska, M.; Jin, F.; Al-Tabbaa, A. Mechanism of reactive magnesia—Ground granulated blastfurnace slag (GGBS) soil stabilization. *Can. Geotech. J.* **2016**, *53*, 773–782. [[CrossRef](#)]
57. Hou, Y.F.; Liu, J.T.; Peng, X.D.; Zhao, S.R. Effect of Iron Tailing Powder Fineness on the Pore Structure of Cement Mortar. *Fly Ash Compr. Util.* **2017**, *5*, 23–26+35.
58. Cui, K.; Chang, J. Hydration, reinforcing mechanism, and macro performance of multi-layer graphene-modified cement composites. *J. Build. Eng.* **2022**, *57*, 104880. [[CrossRef](#)]
59. Ma, H.Z.; Li, Z.Q. Ettringite Formation in Concrete. *Build. Sci.* **2007**, *11*, 105–110. [[CrossRef](#)]
60. Wang, F.S.; Zhu, Y.N.; Ma, J.L.; Sun, R.L. Experimental Research of Sodium Chloride on Activation and Binding Mode of Slag Portland Blend Cement. *Bull. Chin. Ceram. Soc.* **2009**, *28*, 784–791. [[CrossRef](#)]
61. Lu, Q.B.; Yang, Q.B. Influencing factors to activate the potential activity of slag. In Proceedings of the 7th Council Meeting and Academic Exchange Conference of Concrete Cement Products Branch of China Silicate Society, Beijing, China, 19–21 October 2005; Volume 6, pp. 131–134.
62. Liu, S.L.; Li, G.C.; Liu, G.L.; Wang, F.G.; Wang, J. Early Hydration Mechanism of Gypsum Slag-Lime Composite Cementitious System. *Nonferrous Met. Eng.* **2021**, *11*, 102–109. [[CrossRef](#)]
63. Yu, Z.Y.; Zhao, Y.D.; Ba, H.J.; Liu, M.H. Synergistic effects of ettringite-based expansive agent and polypropylene fiber on early-age anti-shrinkage and anti-cracking properties of mortars. *J. Build. Eng.* **2021**, *39*, 102275. [[CrossRef](#)]
64. Hou, D.W. *Integrative Studies on Autogenous and Drying Shrinkage of Concrete and Related Issues*; Tsinghua University: Beijing, China, 2010.
65. Yan, H.D.; Sun, W. Study on the relationship between autogenous shrinkage and drying shrinkage of fly ash mortar. *J. Chin. Ceram. Soc.* **2003**, *31*, 428–433. [[CrossRef](#)]
66. Yuan, B.; Yu, Q.L.; Dainese, E.; Brouwers, H.J.H. Autogenous and drying shrinkage of sodium carbonate activated slag altered by limestone powder incorporation. *Constr. Build. Mater.* **2017**, *153*, 459–468. [[CrossRef](#)]
67. Liu, H.H. *Test Research on Mechanical Performance for Structural Member of Inorganic Polymer Concrete*; Wuhan University of Technology: Wuhan, China, 2014. [[CrossRef](#)]
68. Palacios, M.; Puertas, F. Effect of shrinkage-reducing admixtures on the properties of alkali-activated slag mortars and pastes. *Cem. Concr. Res.* **2007**, *37*, 691–702. [[CrossRef](#)]
69. Taghvayi, H.; Behfarnia, K.; Khalili, M. The Effect of Alkali Concentration and Sodium Silicate Modulus on the Properties of Alkali-Activated Slag Concrete. *J. Adv. Concr. Technol.* **2018**, *16*, 293–305. [[CrossRef](#)]
70. Zhang, B.; Zhu, H.; Cheng, Y.; Ghasan, F.H.; Kwok, W.S. Shrinkage mechanisms and shrinkage-mitigating strategies of alkali-activated slag composites: A critical review. *Constr. Build. Mater.* **2022**, *318*, 125993. [[CrossRef](#)]
71. Zhang, B.; Zhu, H.; Feng, P.; Zhang, P. A review on shrinkage-reducing methods and mechanisms of alkali-activated/geopolymer systems: Effects of chemical additives. *J. Build. Eng.* **2022**, *49*, 104056. [[CrossRef](#)]
72. Yao, J.B.; Yuan, J.; Song, X.F.; Ju, J.T. Influence of Super-absorbent Polymer on the Drying Shrinkage and Cracking of Alkali Activated Slag. *Bull. Chin. Ceram. Soc.* **2019**, *38*, 2335–2339. [[CrossRef](#)]

Disclaimer/Publisher's Note: The statements, opinions and data contained in all publications are solely those of the individual author(s) and contributor(s) and not of MDPI and/or the editor(s). MDPI and/or the editor(s) disclaim responsibility for any injury to people or property resulting from any ideas, methods, instructions or products referred to in the content.